JOURNAL OF GEOPHYSICAL RESEARCH, VOL. 96, NO. B12, PAGES 20,053–20,071, NOVEMBER 10, 1991

On Postglacial Geoid Subsidence Over the Equatorial Oceans

J.X. MITROVICA[1] AND W.R. PELTIER

Department of Physics, University of Toronto, Ontario, Canada

We develop two new spectral formalisms for the gravitationally self-consistent solution of the "sea level equation" which governs the redistribution of glacial meltwater on a visco-elastic Earth. The first is a purely spectral technique based on an extension of theory outlined by Dahlen (1976) for determining the equilibrium oceanic tide on an elastic planet. Using this technique, with a feasible spherical harmonic truncation level ($\ell \leq 30$), we can obtain convergence in the computed sea level variations within the degree range $\ell \leq 10$. We also develop a second, "pseudospectral" technique, however, which permits the construction of gravitationally self-consistent solutions to much higher degree and order ($\ell >> 100$). The pseudospectral formalism is employed here to develop a comprehensive physical explanation for the global pattern of present-day sea level variations due to ongoing glacial isostatic adjustment. In particular, we focus upon a mechanism, which we term "equatorial ocean syphoning," that acts to draw water toward the oceanic portion of the collapsing peripheral bulge that encircles previously glaciated regions. The collapse of the forebulge induces a flow of water which is required to maintain hydrostatic equilibrium. The syphoning mechanism dominates the relative sea level (RSL) variation in oceans in the far field of the ice sheets (that is, beyond the peripheral bulge) during periods, such as the interglacial of the past 4000 years, during which the volume of the ice sheets has not (apparently) changed appreciably, while, at the same time, isostatic adjustment persists. The RSL change in the near field is, in contrast, dominated by the (local) vertical displacement of the solid surface. Finally, comparison of gravitationally self-consistent predictions of RSL change in the far field, with the observational data at small Pacific island sites, has provided an upper bound of 1 to 2 m for the eustatic sea level rise produced by any recent (last 3000 years) melting of the Antarctic ice sheet.

1. INTRODUCTION

Raised and submerged strandlines caused by relative sea level (RSL) change during the last 18,000 ^{14}C years are a manifestation of glacial isostatic adjustment during, and following, the last major deglaciation event of the current ice age. These observations constitute a rather voluminous, globally distributed data set (Tushingham and Peltier, Constraints on visco-elastic Earth structure from a global data base of late Pleistocene relative sea level histories, submitted to *Journal of Geophysical Research*, 1991) that has had application in a variety of geophysical contexts. A comparison of such data with synthetic RSL curves computed using realistic Earth models has provided, and will continue to provide, important constraints upon inferences of mantle viscosity [*Peltier*, 1974; *Cathles*, 1975; *Peltier and Andrews*, 1976; *Wu and Peltier*, 1983; *Mitrovica and Peltier*, 1991]. Furthermore, these comparisons have also been used to construct global models of the late Pleistocene deglaciation history which are significantly better resolved than those based solely on geological constraints [*Wu and Peltier*, 1983; *Tushingham and Peltier*, 1991*a*].

These applications also extend to present-day RSL variations, which have recently received considerable attention in the context of the global warming hypothesis [*Peltier and Tushingham*, 1989]. Scientists seeking evidence for global climate change have turned their attention to the issue of global sea level rise, anticipating that atmospheric warming trends should be manifested in a systematic rise in ocean bathymetry [*Etkins and Epstein*, 1982; *Gornitz et al.*, 1982] caused by the melting of both large and small ice sheets and alpine glaciers. Tide gauge records support the existence of such a trend and this becomes significantly more coherent, globally, when the data are filtered to remove the influence of ongoing glacial isostatic adjustment [*Peltier and Tushingham*, 1989].

Computing the redistribution of ocean water in response to the growth and decay of ice sheets on a realistic Earth is a nontrivial problem. Variations in the ice mass and ocean bathymetry force mass redistributions in the planetary interior which, together with the direct attraction of the surface load (ice plus water), perturb the gravitational field of the planet. It is clear that these perturbations must, in turn, affect the sea level variation since the ocean surface is constrained to remain an equipotential. In mathematical terms this interrelation gives rise to an integral equation, known as the sea level equation [e.g., *Farrell and Clark*, 1976; *Clark et al.* 1978; *Peltier et al.* 1978].

In the past the only gravitationally self-consistent solutions of the equation, for the case of a visco-elastic planet, have been based on a "finite element" formulation described by *Peltier et al.* [1978]. An approximate spectral technique has also been presented [e.g., *Nakiboglu et al.*, 1983]; however, the latter authors assumed that both the potential perturbation due to internal mass redistributions and the deflection of the Earth's solid surface are adequately computed using an ocean load (meltwater) forcing that is independent of geography. In this paper we will present two new techniques for obtaining gravitationally self-consistent solutions of the sea level equation. The first is a "full spectral" formulation based on an extension of theory outlined by *Dahlen* [1976] for the computation of equilibrium tidal heights on an elastic Earth. The procedure is particularly useful for accurately determining the low degree ($\ell \leq 10$) signal of the sea level variation, and we will outline an important application of it that will be pursued in a later publication (section 3.1). The second technique, which we label "pseudospectral," in analogy with similar technology that is employed in modern atmospheric general circulation models, will permit gravitationally self-consistent solutions of the sea level equation to much higher degree and order.

[1]Now at Harvard-Smithsonian, Center for Astrophysics, Cambridge, Massachusetts.

Paper number 91JB01284.
0148-0227/91/91JB-01284$05.00

To demonstrate the utility of the pseudospectral technique we will examine, in some detail, present-day sea level changes due to glacial isostatic adjustment. A primary goal in the analysis is to provide a comprehensive physical theory which can explain the detailed nature of the global pattern of present-day sea level change. As an example, while the fall in sea level near the center of previously glaciated areas, in the last 18,000 years, is obviously a result of the postglacial uplift of the Earth's solid surface in these regions, the physical origin of the present-day sea level fall in oceans in the far field of the ice sheets deduced by *Clark et al.* [1978], *Peltier* [1988] and *Peltier and Tushingham* [1989] may be seen by some as puzzling and in any event deserves a more complete discussion than has been provided to date. Since these authors presented results for only a single Earth model in their analyses, it is not even clear whether the far field sea level fall deduced by them is a feature common to all such models. We will show that it is and that the redistribution of ocean water from the far field is a consequence of the subsidence of the peripheral bulge encircling previously glaciated regions (especially Canada and the Antarctic). We have termed this phenomenon "equatorial ocean syphoning," and its detailed description constitutes, we contend, a useful further contribution to our understanding of the postglacial rebound process.

A second result of the analyses to be presented here lies in the detailed verification of the global signal of the present-day rate of sea level rise computed by *Peltier* [1988] and *Peltier and Tushingham* [1989]. By providing such verification, we provide independent confirmation of the validity and accuracy of the previously employed finite element formulation for the solution of the sea level equation [*Peltier et al.* 1978] and, by implication, strengthen the many important conclusions that have been based upon its application.

2. The Sea Level Equation

The accumulation and ablation of Pleistocene ice sheets, together with the complimentary variation in ocean bathymetry, constitute the surface load which drives the glacial isostatic adjustment process. For a fixed ice load history and visco-elastic Earth model a gravitationally self-consistent calculation of the space and time dependent changes in ocean bathymetry requires the solution of the sea level equation. In this section we will outline its derivation for the case of a spherically symmetric (in its unperturbed state) visco-elastic planet [after *Farrell and Clark*, 1976; *Clark et al.*, 1978; *Peltier et al.*, 1978] with the intent of illustrating the basic physical principles which govern the redistribution of ocean water.

The gravitational potential perturbation $\Phi(\theta, \psi, t)$ on the Earth's original unperturbed surface, produced by a general surface load $L(\theta, \psi, t)$, can be computed via the space-time convolution

$$\Phi(\theta,\psi,t) = \int_{-\infty}^{t} \iint_{\Omega} L(\theta',\psi',t')\, \phi(\gamma, t-t')\, d\Omega'\, dt', \qquad (1)$$

where Ω represents the entire surface area of the Earth, γ is the angular distance from (θ, ψ) to (θ', ψ'), and ϕ is the potential perturbation Green function [*Peltier and Andrews*, 1976]. The geoid anomaly, that is the change in position of the sea level surface relative to the reference ellipsoid, is related to Φ by

$$G(\theta,\psi,t) = \left(\Phi(\theta,\psi,t) + \Delta\Phi(t)\right)/g, \qquad (2)$$

where g is the surface gravitational acceleration. The inclusion of the term labelled $\Delta\Phi$ reflects the fact that the particular equipotential upon which the sea level lies will not in general be constant in time.

In analogy with equation (1) the radial displacement of the solid surface produced by the surface load is

$$R(\theta,\psi,t) = \int_{-\infty}^{t} \iint_{\Omega} L(\theta',\psi',t')\, \Gamma(\gamma, t-t')\, d\Omega'\, dt', \qquad (3)$$

where $\Gamma(\gamma, t)$ is the radial displacement Green function [*Peltier*, 1974]. The sea level change is simply the difference between the geoidal and solid surface perturbations at geographic positions coincident with the oceans. Accordingly,

$$\begin{aligned} S(\theta,\psi,t) &= C(\theta,\psi)\left\{G(\theta,\psi,t) - R(\theta,\psi,t)\right\} \\ &= C(\theta,\psi)\left[\int_{-\infty}^{t} \iint_{\Omega} L(\theta',\psi',t') \times \left\{\frac{\phi(\gamma,t-t')}{g} - \Gamma(\gamma,t-t')\right\} d\Omega'\, dt' + \frac{\Delta\Phi(t)}{g}\right] \end{aligned} \qquad (4)$$

where $S(\theta, \psi, t)$ is the sea level variation, and $C(\theta, \psi)$ is the ocean function defined as [*Munk and MacDonald*, 1960]

$$\begin{aligned} C(\theta,\psi) &= 1 \quad \text{in the oceans} \\ C(\theta,\psi) &= 0 \quad \text{elsewhere} \end{aligned} \qquad (5)$$

The value of the constant $\Delta\Phi$ is chosen in order to ensure that the sea level change conserves mass. Its value (via equation (2)) is chosen to force the total volume between the three dimensional geoidal and solid Earth surfaces to be equal to the volume of water exchanged between the ice sheets and the oceans. Using equation (4) we have

$$\frac{\Delta\Phi(t)}{g} = -\frac{M_I(t)}{\rho_w A_o} - \frac{1}{A_o}\left\langle \int_{-\infty}^{t} \iint_{\Omega} L(\theta',\psi' t') \cdot \left\{\frac{\phi(\gamma,t-t')}{g} - \Gamma(\gamma,t-t')\right\} d\Omega'\, dt' \right\rangle \qquad (6)$$

where M_I is the mass loss history of the ice sheets, ρ_w is the density of water, A_o is the area of the oceans (which is assumed constant, though $C(\theta, \psi)$ will actually depend slightly on sea level), and angle brackets denote integration over the oceans. The first term on the R.H.S of equation (6) is referred to as the eustatic sea level change. It represents the variation in bathymetry that would be measured if the distribution of water added to, or removed from, the oceans was independent of geographic location (and the original ocean mass was fixed to the spatial distribution that obtained prior to the onset of melting). The second term on the right-hand side is an integrated measure of the distance between the equipotential which originally coincided with sea level and the Earth's solid surface.

The Green functions $\phi(\gamma, t)$ and $\Gamma(\gamma, t)$ can be expressed in terms of the surface load Love numbers defined by *Peltier* [1974], for the surface loading of a visco-elastic planet. In the time domain the h and k Love numbers have the following forms [*Peltier*, 1976]:

$$h_\ell(t) = h_\ell^E \delta(t) + \sum_{k=1}^{K} r_k^\ell \exp(-s_k^\ell t)$$

$$k_\ell(t) = k_\ell^E \delta(t) + \sum_{k=1}^{K} r'^\ell_k \exp(-s_k^\ell t). \quad (7)$$

These numbers represent the (nondimensional) spherical harmonic (degree ℓ) coefficients in the Legendre polynomial expansion of the Green functions for radial displacement (h_ℓ) and the potential perturbation due to mass redistribution in the planetary interior (k_ℓ). We have employed the method developed by *Peltier* [1985] for their computation.

Using equation (7), restored to dimensional form, we have

$$\phi^{MR}(\gamma,t) = \frac{ag}{M_e}\sum_{\ell=o}^{\infty}\left\{k_\ell^E\delta(t)+\sum_{k=1}^{K} r'^\ell_k exp(-s_k^\ell t)\right\} P_\ell(\cos\gamma)$$

$$\Gamma(\gamma,t) = \frac{a}{M_e}\sum_{\ell=o}^{\infty}\left\{h_\ell^E\delta(t)+\sum_{k=1}^{K} r_k^\ell exp(-s_k^\ell t)\right\} P_\ell(\cos\gamma) \quad (8)$$

where the P_ℓ are Legendre polynomials, and the superscript MR refers to the internal mass redistribution contribution to the total potential perturbation. M_e and "a" are the Earth's mass and radius, respectively. The potential perturbation Green function ϕ in equation (1) also has a contribution from the direct attraction of the load, and we can write [e.g., *Farrell*, 1972]

$$\phi(\gamma,t) = \phi^{MR}(\gamma,t) + \phi^{L}(\gamma,t) \quad (9a)$$

where

$$\phi^{L}(\gamma,t) = \frac{ag}{M_e}\sum_{\ell=o}^{\infty} P_\ell(\cos\gamma)\,\delta(t). \quad (9b)$$

Using equations (8) and (9), the time dependent constant $\Delta\Phi(t)/g$ can then be expressed as the combination

$$\frac{1}{g}\Delta\Phi(t) = \zeta(t) - \frac{1}{g}\Delta\Phi^{L}(t) - \frac{1}{g}\Delta\Phi^{MR}(t) + \frac{1}{g}\Delta\Phi^{\Gamma}(t), \quad (10)$$

where

$$\zeta(t) = -\frac{M_I(t)}{\rho_w A_o}$$

$$\frac{1}{g}\Delta\Phi^{L}(t) = \frac{1}{A_o}\left\langle\int_{-\infty}^{t}\iint_{\Omega} L(\theta',\psi',t')\frac{1}{g}\phi^{L}(\gamma,t-t')\,d\Omega'\,dt'\right\rangle$$

$$\frac{1}{g}\Delta\Phi^{MR}(t) = \frac{1}{A_o}\left\langle\int_{-\infty}^{t}\iint_{\Omega} L(\theta',\psi',t')\frac{1}{g}\phi^{MR}(\gamma,t-t')\,d\Omega'\,dt'\right\rangle$$

$$\frac{1}{g}\Delta\Phi^{\Gamma}(t) = \frac{1}{A_o}\left\langle\int_{-\infty}^{t}\iint_{\Omega} L(\theta',\psi',t')\,\Gamma(\gamma,t-t')\,d\Omega'\,dt'\right\rangle. \quad (11)$$

We will see that the different time dependent terms in equation (10) constitute important diagnostics in the investigation of the physical cause of meltwater redistribution over the ocean basins subsequent to deglaciation.

Returning to equation (4), the surface load L can be separated into contributions from the ice sheets and from the associated sea level variations, and as a consequence a computation of $S(\theta,\psi,t)$ must involve the solution of an integral equation. If we denote by I the thickness of ice, then

$$L(\theta,\psi,t) = \rho_I I(\theta,\psi,t) + \rho_w S(\theta,\psi,t), \quad (12)$$

where ρ_I is the density of ice. Using equation (12) in equation (4) we then have

$$S(\theta,\psi,t) = C(\theta,\psi)\left[\int_{-\infty}^{t}\iint_{\Omega}\left(\rho_I I(\theta',\psi',t') + \rho_w S(\theta',\psi',t')\right)\cdot\left\{\frac{1}{g}\phi(\gamma,t-t') - \Gamma(\gamma,t-t')\right\}d\Omega'\,dt' + \frac{\Delta\Phi(t)}{g}\right]. \quad (13)$$

Equation (13) is the general sea level equation for the case of a visco-elastic planet. To solve it generally requires a discretization in time, and it has been common [*Farrell and Clark*, 1976; *Peltier and Andrews*, 1976; *Clark et al.*, 1978; *Wu and Peltier*, 1983] to model the ice load (and subsequent sea level change) as a series of step load increments. Accordingly, we can write

$$I(\theta,\psi,t) = \sum_{n=o}^{N}\delta I^n(\theta,\psi)\,H(t-t_n)$$

$$S(\theta,\psi,t) = \sum_{n=o}^{N}\delta S^n(\theta,\psi)\,H(t-t_n) \quad (14)$$

in which H(t) is the Heaviside step function. The special form of equation (14) permits an analytic solution for the time convolution in equation (13). Using equations (8), (9), (13), and (14), one can show that

$$\sum_{n=o}^{N}\delta S^n(\theta,\psi)\,H(t-t_n) = C(\theta,\psi)\left[\frac{\Delta\Phi(t)}{g} + \iint_{\Omega}\left\{\rho_I(\theta',\psi',t) + \rho_w S(\theta',\psi',t)\right\}S^E(\gamma)\,d\Omega' + \sum_{n=o}^{N}H(t-t_n)\iint_{\Omega}\left\{\rho_I\delta I^n(\theta',\psi') + \rho_w\delta S^n(\theta',\psi')\right\}\cdot S^{NE}(\gamma,t)\,d\Omega'\right] \quad (15)$$

in which

$$S^E(\gamma) = \sum_{\ell=o}^{\infty}\frac{a}{M_e}E_\ell P_\ell(\cos\gamma)$$

$$S^{NE}(\gamma,t) = \sum_{\ell=o}^{\infty}\frac{a}{M_e}\beta(\ell,t_n,t)\,P_\ell(\cos\gamma) \quad (16)$$

where

$$E_\ell = 1 + k_\ell^E - h_\ell^E$$

$$\beta(\ell,t_n,t) = \sum_{k=1}^{K}\frac{(r'^\ell_k - r_k^\ell)}{s_k^\ell}\left[1-\exp(-s_k^\ell(t-t_n))\right].$$

The second and third terms on the right-hand side of equation (15) represent the elastic and nonelastic responses, respectively, in the convolution of the full surface load with the Green function $\phi(\gamma, t)/g\Gamma(\gamma, t)$. The Green functions S^E and S^{NE}, since they incorporate a convolution with the time history (14), have come to be known as Heaviside Green functions [*Peltier and Andrews*, 1976]. In equation (15) the partition of $\Delta\Phi(t)$, as defined in equations (10) and (11), follows directly from a simple division of E_ℓ into contributions from the load (1.0), internal mass redistribution (k_ℓ^E) and solid Earth deformation ($-h_\ell^E$).

The sea level variation $S(\theta, \psi, t)$ is computed, using equation (15), by solving for successive increments $\delta S^n(\theta, \psi)$. To date the only gravitationally self-consistent solutions of the equation have been based on the finite element formulation described by *Peltier and Andrews* [1976], *Peltier et al.* [1978], and *Wu and Peltier* [1983]. In this technique the ice and ocean surfaces were discretized using circular discs of varying radius (the resolution is generally maximized at continental shorelines), and the convolution over the Earth's surface is performed, in the space domain, using a large set of precomputed interaction coefficients (the finite element classification adopted by the authors is somewhat unconventional since the methodology incorporates elements of both Green function and finite element techniques). For each sea level increment the solution is obtained iteratively, and the first guess is given by the eustatic sea level change,

$$[\delta S^n(\theta,\psi)]^{i+1} = -\rho_I \left\{ \iint_\Omega \delta I^n(\theta,\psi)\, d\Omega \right\} \frac{C(\theta,\psi)}{\rho_w A_o}. \quad (17)$$

The process continues until convergence, defined by the level of consistency obtained in equation (15), is established.

In the following sections we shall outline two new approaches for generating solutions to the sea level equation (15). Both techniques are based upon a spectral formulation of the required surface convolution integrals. As a consequence, and in contrast to the finite element approach described above, the resolution will be more uniform around the globe, and dependent upon the truncation level of the various spherical harmonic expansions. In this respect, the methodology we have developed will feasibly allow for gravitationally self-consistent solutions to very large (>> 100) spherical harmonic degree and order.

3. Solving the Sea Level Equation: Spectral Approaches

Any field $\chi(\theta, \psi)$, defined on the surface of the sphere, can be represented in terms of a spherical harmonic expansion of the form

$$\chi(\theta,\psi) = \sum_{\ell=o}^{\infty} \sum_{m=-\ell}^{\ell} \chi_{\ell m} Y_{\ell m}(\theta,\psi), \quad (18)$$

where the $Y_{\ell m}$ are surface spherical harmonics normalized (in our calculations) such that

$$\iint_{SPHERE} Y_{\ell' m'}(\theta,\psi)\, Y^*_{\ell m}(\theta,\psi)\, \sin\theta\, d\theta\, d\psi = 4\pi\, \delta_{\ell\ell'}\, \delta_{mm'}. \quad (19)$$

The asterisk denotes complex conjugation. In this case one can show that

$$\iint_\Omega \chi(\theta,\psi)\, P_\ell(\cos\gamma)\, d\Omega' = \frac{4\pi a^2}{(2\ell+1)} \sum_{m=-\ell}^{\ell} \chi_{\ell m} Y_{\ell m}(\theta,\psi). \quad (20)$$

Therefore if we denote the spherical harmonic coefficients of the ocean function (equation (5)), the total ice load and sea level variation (equation (12)), and the ice and sea level increments (equation (14)) by $C_{\ell m}$, $I_{\ell m}$, $S_{\ell m}$, $\delta I^n_{\ell m}$ and $\delta S^n_{\ell m}$, respectively, the sea level equation (15) can be written as

$$\sum_{\ell=o}^{\infty} \sum_{m=-\ell}^{\ell} + S_{\ell m}(t)\, Y_{\ell m}(\theta,\psi) = \left(\sum_{r=o}^{\infty} \sum_{s=-r}^{r} C_{rs} Y_{rs}(\theta,\psi) \right)$$

$$\left[\frac{\Delta\Phi(t)}{g} + \sum_{\ell=o}^{\infty} \sum_{m=-\ell}^{\ell} E_\ell T_\ell \left(\rho_I I_{\ell m}(t) + \rho_w S_{\ell m}(t) \right) Y_{\ell m}(\theta,\psi) \right.$$

$$+ \sum_{\ell=o}^{\infty} \sum_{m=-\ell}^{\ell} T_\ell \sum_{n=o}^{N} \left(\rho_I \delta I^n_{\ell m} + \rho_w \delta S^n_{\ell m} \right) \cdot$$

$$\left. \cdot \beta(\ell, t_n, t)\, H(t - t_n)\, Y_{\ell m}(\theta,\psi) \right] \quad (21)$$

where

$$T_\ell = \frac{4\pi a^3}{M_e(2\ell+1)}. \quad (22)$$

Using this formalism we can derive a particularly simple relation between the degree zero component of the ice and ocean load. Conservation of mass requires that

$$\iint_\Omega L(\theta,\psi,t)\, d\Omega = 0. \quad (23)$$

Using equations (12), (14), (18) and (19), it is easy to show that equation (23) implies

$$\rho_I I_{oo}(t) + \rho_w S_{oo}(t) = 0$$

$$\rho_I \delta I^n_{oo} + \rho_w \delta S^n_{oo} = 0. \quad (24)$$

We will consider two different approaches to the solution of the integral equation (21). In the first we derive a purely spectral formalism based on an extension, to the visco-elastic case, of theory outlined by *Dahlen* [1976] for determining the equilibrium oceanic tide of an elastic planet.

3.1. A "Full Spectral" Approach

Let us seek a solution for the sea level variation at a time $t = t_j$, coinciding with the application of the $(j+1)^{st}$ ice load increment. Using the spectral form of equation (14) we can write

$$\delta S^j_{\ell m} = S_{\ell m}(t_j) - S_{\ell m}(t_{j-1}). \quad (25)$$

If we assume that $S_{\ell m}(t_{j-1})$ has been solved for in a previous time step, then our problem reduces to computing $\delta S^j_{\ell m}$. Applying

equation (25) to equation (21) yields

$$\sum_{\ell,m} \delta S^j_{\ell m} Y_{\ell m} = -\sum_{\ell,m} S_{\ell m}(t_{j-1}) Y_{\ell m} + \left\{\sum_{r,s} C_{rs} Y_{rs}\right\} \cdot$$

$$\left[\frac{\Delta\Phi}{g}(t_j) + \sum_{\ell,m} E_\ell T_\ell \left(\rho_I I_{\ell m}(t_j) + \rho_w (S_{\ell m}(t_{j-1}) + \rho_w \delta S^j_{\ell m}\right) Y_{\ell m}\right.$$

$$\left. + \sum_{\ell,m} T_\ell \sum_{n=o}^{j-1} \beta(\ell, t_n, t_j)\left(\rho_I \delta I^n_{\ell m} + \rho_w \delta S^n_{\ell m}\right) Y_{\ell m}\right] \qquad (26)$$

where

$$\sum_{\ell,m} \equiv \sum_{\ell=o}^{\infty} \sum_{m=-\ell}^{\ell}, \quad Y_{\ell m} \equiv Y_{\ell m}(\theta, \psi).$$

Dahlen [1976], in an analysis of the response of an elastic Earth to a static tidal potential, derived an equation similar in form to equation (26). As is standard in any Galerkin procedure we proceed by multiplying both sides of the equation by $Y^*_{pq}(\theta, \psi)$ and then integrating over the Earth's surface. The result, using equation (19), is the system of algebraic equations:

$$\delta S^j_{pq} - \frac{1}{4\pi} \sum_{\ell,m} M1^{qm}_{p\ell} E_\ell T_\ell \rho_w \delta S^j_{\ell m} = -S_{pq}(t_{j-1}) + C_{pq} \frac{\Delta\Phi(t_j)}{g} +$$

$$+ \frac{1}{4\pi} \sum_{\ell,m} M1^{qm}_{p\ell} E_\ell T_\ell \{\rho_I I_{\ell m}(t_j) + \rho_w S_{\ell m}(t_{j-1})\}$$

$$+ \frac{1}{4\pi} \sum_{\ell,m} M1^{qm}_{p\ell} T_\ell \sum_{n=o}^{j-1} \beta(\ell, t_n, t_j)\left\{\rho_I \delta I^n_{\ell m} + \rho_w \delta S^n_{\ell m}\right\} \qquad (27)$$

in which

$$M1^{qm}_{p\ell} = \sum_{r,s} C_{rs} \iint_{SPHERE} Y^*_{pq} Y_{rs} Y_{\ell m} \sin\theta d\theta d\psi. \qquad (28)$$

The surface integral in equation (28) can be expressed in terms of a product of Wigner 3-j symbols. If we define the inner product

$$\iint_{SPHERE} Y^*_{pq} Y_{rs} Y_{\ell m} \sin\theta d\theta\, d\psi \equiv A^{qsm}_{pr\ell} \qquad (29)$$

then [*Cohen-Tannoudji et al.*, 1977]

$$A^{qsm}_{pr\ell} = (-1)^q 4\pi \left((2p+1)(2r+1)(2\ell+1)\right)^{1/2} \cdot$$

$$\cdot \begin{bmatrix} p & r & \ell \\ 0 & 0 & 0 \end{bmatrix} \begin{bmatrix} p & r & \ell \\ -q & s & m \end{bmatrix} \qquad (30)$$

where the square brackets represent the Wigner 3-j symbol. It follows from the properties of these symbols that $A^{qsm}_{pr\ell}$ vanishes unless all of the following conditions are met:

$$q = s + m$$

$$p + r + \ell \text{ is even}$$

$$|p - \ell| \le r \le p + \ell \qquad (31)$$

Applying these conditions to equation (28) yields

$$M1^{qm}_{p\ell} = \sum_{\substack{r=|p-\ell| \\ r \ge |q-m|}}^{p+\ell}{}_{,2} C_{r,q-m} A^{q\ q-m\ m}_{p\ r\ \ell} \qquad (32)$$

where the subscript on the summation indicates that only every second term is included. Equation (32) ensures that only a finite number of terms are required to compute M1 for a given p, q, ℓ, and m. In this respect the relation (30) is important given the recent derivation of general, and very efficient, recursion formulae for the computation of the 3-j symbols [*Le Blanc*, 1987].

Equation (27) represents an infinite set of coupled linear equations, and therefore any practical scheme for its solution requires that a specific truncation level be chosen. If we assume that the harmonic coefficients of the ice load and sea level vanish for spherical harmonic degree above the value D_{MAX}, then the number of equations in the system is

$$\sum_{D=0}^{D_{MAX}} (2D+1) = D_{MAX}(D_{MAX}+2) + 1. \qquad (33)$$

This is also the number of unknowns (δS^n_{pq} for $p \ge 1$, since δS^n_{oo} is constrained by equation (24), and $\Delta\Phi(t_j)$), and therefore there is a single unique solution to the equation.

To generate the solution, let us first note that the summations over degree ℓ in equation (27) will, in fact, begin at $\ell = 1$ since the degree zero terms cancel as a consequence of the conservation of mass constraint (24). To proceed, we partition the set of equations into those for p=0 (a single equation) and p>0. For the sake of brevity we will write the equations in vector notation, using the convention that any set of coefficients χ_{pq}, for p>0, will be denoted as χ. The vector χ has elements ($\chi_{1\text{-}1}$, χ_{10}, χ_{11}, $\chi_{2\text{-}2}$, ...). Furthermore, we define the matrix [M1], the vector **M0**, and the diagonal matrices [E], [**T**], and $[\beta^j_n]$ to have the following elements:

$$[M1] = \begin{bmatrix} M1^{-1-1}_{1\ 1} & M1^{-1\ 0}_{1\ 1} & M1^{-1\ 1}_{1\ 1} & M1^{-1-2}_{1\ 2} & \cdots \\ M1^{0-1}_{1\ 1} & M1^{0\ 0}_{1\ 1} & M1^{0\ 1}_{1\ 1} & M1^{0-2}_{1\ 2} & \cdots \\ M1^{1-1}_{1\ 1} & M1^{1\ 0}_{1\ 1} & M1^{1\ 1}_{1\ 1} & M1^{1-2}_{1\ 2} & \cdots \\ M1^{-2-1}_{2\ 1} & M1^{-2\ 0}_{2\ 1} & M1^{-2\ 1}_{2\ 1} & M1^{-2-2}_{2\ 2} & \cdots \\ \cdot & \cdot & \cdot & \cdot & \cdot \\ \cdot & \cdot & \cdot & \cdot & \cdot \\ \cdot & \cdot & \cdot & \cdot & \cdot \end{bmatrix} \qquad (34)$$

$$MO = \left[M1^{0-1}_{0\ 1}, M1^{0\ 0}_{0\ 1}, M1^{0\ 1}_{0\ 1}, M1^{0-2}_{0\ 2}, \cdots\right],$$

$$[E] = diag[E_1, E_1, E_1, E_2, \cdots],$$

$$[T] = diag[T_1, T_1, T_1, T_2, \cdots],$$

$$[\beta^j_n] = diag[\beta(1,t_n,t_j), \beta(1,t_n,t_j), \beta(1,t_n,t_j), \beta(2,t_n,t_j), \cdots].$$

Using this notation, the case p>0 in equation (27) becomes

$$\delta S^j = \left\{ [1] - \frac{\rho_w}{4\pi} [M1][E][T] \right\}^{-1} \left[-S(t_{j-1}) + C \frac{\Delta\Phi(t_j)}{g} + \frac{1}{4\pi}[M1][T]\left\{ [E]\left(\rho_I I(t_j) + \rho_w S(t_{j-1})\right) + \sum_{n=o}^{j-1} [\beta_n^j]\left(\rho_I \delta I^n + \rho_w \delta S^n\right) \right\} \right] \quad (35)$$

where [1] denotes the identity matrix. Furthermore, the case p=0 yields (using equation (24))

$$\frac{C_{oo}}{g}\Delta\Phi(t_j) = -\frac{\rho_I}{\rho_w} I_{oo}(t_j) - \frac{\rho_w}{4\pi} MO[E][T]\delta S^j - \frac{1}{4\pi} MO[T]\left\{ [E]\left(\rho_I I(t_j) + \rho_w S(t_{j-1})\right) + \sum_{n=o}^{j-1} [\beta_n^j]\left(\rho_I \delta I^n + \rho_w \delta S^n\right) \right\} \quad (36)$$

By substituting equation (35) into the right-hand side of equation (36), one can solve for $\Delta\Phi(t_j)$. Using this value in equation (35) yields the vector δS^j containing the spherical harmonic coefficients of the $(j+1)^{st}$ sea level increment; that is, the required solution of the sea level equation.

The inversion in equation (35) can be performed extremely efficiently by taking advantage of the diagonally dominant nature of the matrix [e.g., *Dahlen*, 1976]. As a consequence, the main computational effort in the solution for δS^j is focussed on the generation of the matrix [M1]. This effort can be reduced substantially by using the recursion algorithm for the Wigner 3-j symbols derived by *Le Blanc* [1987], and by recognizing the inherent symmetries in the matrix [M1]. For example,

$$M1_{\ell p}^{mq} = M1_{p\ell}^{qm*} \quad (37)$$

$$M1_{p\ell}^{-q-m} = \sum_{\substack{r=|p-\ell| \\ r\geq|q-m|}}^{p+\ell}{}_{,2}\, C_{r,q-m}^{*} (-1)^{q-m} A_p^{q}{}_{r}^{q-m}{}_{\ell}^{m}. \quad (38)$$

Nevertheless, since the operation count required to compute [M1] (see equations (30) and (32)) approximately doubles every three degrees, we have found that truncation levels beyond about degree 30 rapidly become unfeasible. Unfortunately, although asymptotic expressions for the 3-j symbols at large and unequal degrees have been sought, there is reason to believe that they do not exist [*Brussaard and Tolhoek*, 1957].

A truncation level of 30 is not sufficient to accurately compute most RSL curves, especially near irregular ice sheet perimeters and continental margins. However, glacial isostatic disequilibrium is also manifested in the global gravity field, and, in particular, attention has been recently focussed on the low-degree zonal components in the present-day secular variation of the Earth's geoid (the so-called $\dot{J}_\ell$, for $\ell \leq 4$; *Peltier* [1983, 1985] (for ℓ=2), *Mitrovica and Peltier*, [1989]). In section 4.1 we will show that calculations of $\delta S_{\ell m}$, for $\ell \leq 10$, using the methodology outlined in this section, will have converged for truncation levels at degree 30. Hence a gravitationally self-consistent prediction of the $\dot{J}_\ell$ at these low degrees can be obtained using the surface load generated from the "full spectral" approach outlined here (see section 4.1).

A major goal of the present study, however, is to examine the nature and cause of present day RSL variations in the global oceans. We are obliged therefore to seek a technique which permits a much higher truncation level, and in the next section we introduce a pseudospectral formalism for the solution of the sea level equation which satisfies this requirement.

3.2. *A Pseudospectral Approach*

Let us return once more to a consideration of equation (26). If we define

$$R_{pq}(t_j) = E_p T_p \left(\rho_I I_{pq}(t_j) + \rho_w S_{pq}(t_{j-1}) + \rho_w \delta S_{pq}^j\right) + T_p \sum_{n=o}^{j-1} \beta(p, t_n, t_j)\left(\rho_I \delta I_{pq}^n + \rho_w \delta S_{pq}^n\right) \quad (39)$$

then we can rewrite equation (26) in the form

$$\sum_{\ell,m} \delta S_{\ell m}^j Y_{\ell m} = -\sum_{\ell,m} S_{\ell m}(t_{j-1}) Y_{\ell m} + \left\{ \sum_{r,s} C_{rs} Y_{rs} \right\} \cdot \left[\sum_{p,q} R_{pq}(t_j) Y_{pq} + \frac{\Delta\Phi}{g}(t_j) \right]. \quad (40)$$

A comparison with equation (25) indicates that the second term on the right-hand side of equation (40) represents the sea level change up to time t_j (that is, $S(\theta, \psi, t_j)$). This term represents a projection of the field measuring the distance between the sea level equipotential and the solid surface onto the ocean function.

In the last section this projection was performed spectrally. The inner product which was then applied to solve for $\delta S_{\ell m}^j$ (equation (27)) produced elements of the form (28) whose generation ultimately limited the truncation level. This suggests that it may be more efficient to perform the projection in the space domain, and in this section we outline a simple, iterative, technique based on this idea.

Let us consider that an approximation to the spherical harmonic coefficients of the sea level increment δS^j (equation (14)) exists. If we denote this approximation as $[\delta S_{\ell m}^j]^i$, then equation (40) provides an algorithm for its (iterative) improvement. In particular, if we denote the "improved" estimate as $[\delta S_{\ell m}^j]^{i+1}$, then we may write, using equation (40),

$$\sum_{\ell,m} [\delta S_{\ell m}^j]^{i+1} Y_{\ell m} = -\sum_{\ell,m} S_{\ell m}(t_{j-1}) Y_{\ell m} + \left\{ \sum_{r,s} C_{rs} Y_{rs} \right\} \cdot \left[\sum_{p,q} [R_{pq}(t_j)]^i Y_{pq} + \left[\frac{\Delta\Phi(t_j)}{g} \right]^i \right] \quad (41)$$

where, using equation (39),

$$[R_{pq}(t_j)]^i = E_p T_p \left(\rho_I I_{pq}(t_j) + \rho_w S_{pq}(t_{j-1}) + \rho_w [\delta S_{pq}^j]^i\right) + T_p \sum_{n=o}^{j-1} \beta(p, t_n, t_j)\left(\rho_I \delta I_{pq}^n + \rho_w \delta S_{pq}^n\right). \quad (42)$$

It will be instructive to define the function,

$$R^i(\theta,\psi,t_j) = \sum_{p,q} [R_{pq}(t_j)]^i Y_{pq}. \quad (43)$$

If we furthermore define the projection

$$RO^i(\theta,\psi,t_j) = \left\{\sum_{r,s} C_{rs} Y_{rs}\right\} \cdot \left[\sum_{p,q} [R_{pq}(t_j)]^i Y_{pq}\right], \quad (44)$$

then, using equation (43), we have

$$RO^i(\theta,\psi,t_j) = C(\theta,\psi)\, R^i(\theta,\psi,t_j). \quad (45)$$

The spherical harmonic expansion of $RO^i(\theta,\psi,t_j)$ can be represented by

$$RO^i(\theta,\psi,t_j) = \sum_{l,m} [RO_{lm}(t_j)]^i Y_{lm}. \quad (46)$$

Using equations (45) and (46) in (41) yields the spectral equation

$$[\delta S^j_{lm}]^{i+1} = -S_{lm}(t_{j-1}) + [RO_{lm}(t_j)]^i + \left[\frac{\Delta\Phi(t_j)}{g}\right]^i C_{lm}. \quad (47)$$

The term $[\Delta\Phi(t_j)/g]^i$ can be derived by enforcing conservation of mass on the terms in equation (40). This yields, using equations (14), (45), and (46),

$$\left[\frac{\Delta\Phi(t_j)}{g}\right]^i = \left(-\frac{\rho_I}{\rho_w} I_{oo}(t_j) - [RO_{oo}(t_j)]^i\right)(C_{oo})^{-1}. \quad (48)$$

Equations (42)-(48) provide the basis for the iterative pseudo-spectral solution to the sea level equation to be described in this section (and implemented in section 4.2). In this respect, the parameter i represents the iteration counter.

The algorithm for the pseudospectral technique is summarized in Figure 1. To begin, the ocean function is specified at N latitude and M longitude points (a total of N x M nodes). Furthermore, a first guess to the spherical harmonic coefficients of the sea level increment, $[\delta S^j_{lm}]^{i=1}$, is also specified, and, using equation (42), the coefficients $[R_{pq}(t_j)]^{i=1}$ are generated. From these coefficients the field $R^{i=1}(\theta, \psi, t_j)$ can be synthesized at the same N x M nodes (as expressed in equation 43), and the product (or projection) of $R^{i=1}(\theta, \psi, t_j)$ and the ocean function $C(\theta, \psi)$ (as required in equation 45) computed at each. The result, $RO^{i=1}(\theta, \psi, t_j)$, is then decomposed to generate the coefficients $[RO_{lm}(t_j)]^{i=1}$. Using $[RO_{oo}(t_j)]^{i=1}$ in equation (48) yields the term $[\Delta\Phi(t_j)/g]^{i=1}$. The entire RHS of equation (47) is thus established, and the next sea level increment $[\delta S^j_{lm}]^{i=2}$ can be computed. The procedure is repeated (compute $[R_{pq}(t_j)]^{i=2}$, etc...) until convergence is obtained.

The first guess to the sea level increment is the eustatic change. Using equations (17), (19), and (24) we have

$$[\delta S^j_{lm}]^{i-1} = -\left\{\frac{\rho_I}{\rho_w}\frac{4\pi a^2}{A_o}\delta I^j_{oo}\right\} C_{lm}. \quad (49)$$

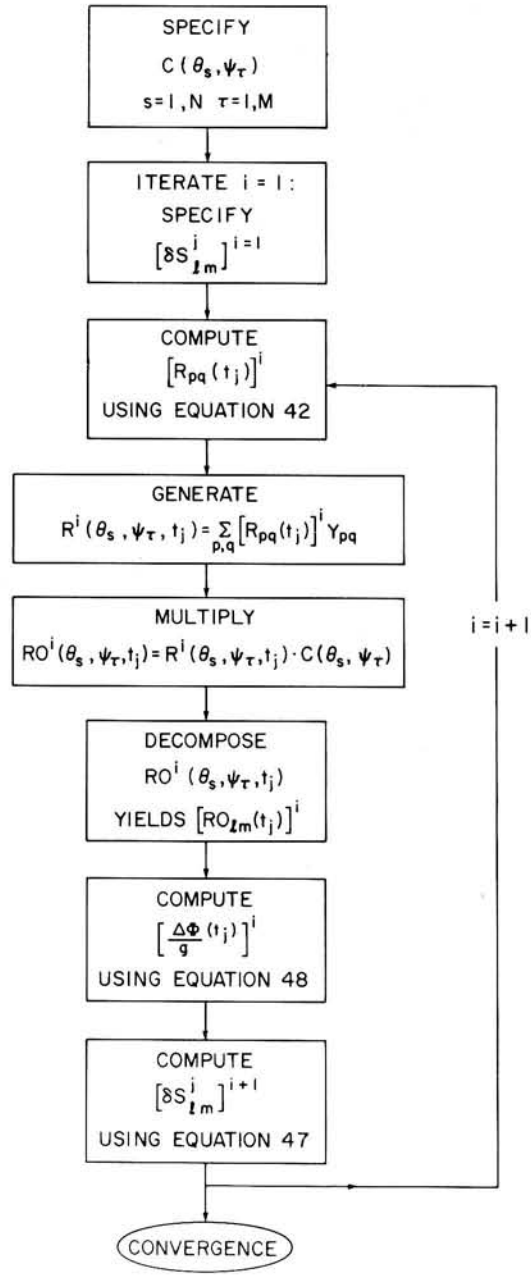

Fig. 1. A pseudospectral solution to the sea level equation.

Furthermore, the level of convergence may be assessed by computing

$$\xi^{i+1} = \sum_{l,m} \frac{|[\delta S^j_{lm}]^{i+1}| - |[\delta S^j_{lm}]^i|}{|[\delta S^j_{lm}]^i|} \quad (50)$$

where the vertical bars represent the modulus of the complex variable. We have found that three of four iterations are sufficient to assure that $\xi < 10^{-4}$.

We have labelled the technique pseudo-spectral because all computations are performed in the spectral domain, with the exception of the projection of $R^i(\theta, \psi, t_j)$ onto the ocean function. The procedure of transforming to the space domain, calculating the projection, and then returning to the spectral domain, can be performed extremely efficiently (the technique is common in general circulation models of the Earth's atmosphere; [e.g., *Laprise*, 1981]). The spherical harmonic coefficients are computed

by first applying a Fast Fourier Transform to the longitudinal nodal values along a fixed latitude circle, and then integrating, using Gaussian quadrature, over colatitude. Resynthesizing a field from the coefficients involves a simple summation over degree, for fixed order, followed by an inverse Fourier transform. The number of nodes used is, of course, dependent on the spherical harmonic truncation level.

This technique represents a fundamentally different approach to generating gravitationally self-consistent solutions of the sea level equation than that embodied in previous finite element models. It avoids, for example, complicated spatial convolutions (see equation (16)) and gridding schemes. Furthermore, it extends the possible spherical harmonic truncation level well beyond the degree 30 range of the "full spectral" formalism introduced in section 3.1. In section 4.2 we present results for calculations of present-day RSL variations based upon truncation at spherical harmonic degree 128. We must stress, however, that higher truncation levels are certainly feasible.

3.3. Other Spectral Approaches

The full spectral and pseudospectral formalisms described above yield gravitationally self-consistent solutions of the sea level equation (13). The necessity of solving an integral equation can, however, be avoided by applying certain approximations. As an example, *Nakiboglu et al.* [1983] describe a technique which assumes that the meltwater loads the oceans eustatically. Using this approximation on the right-hand side of our equation (21) yields

$$\sum_{\ell,m} S'_{\ell m}(t) Y_{\ell m} = \left\{ \sum_{r,s} C_{rs} Y_{rs} \right\} \left[\frac{\Delta \Phi^E(t)}{g} + \sum_{\ell,m} E_\ell T_\ell \left(\rho_I I_{\ell m}(t) + \rho_w S^E_{\ell m}(t) \right) Y_{\ell m} + \sum_{\ell,m} T_\ell \sum_{n=o}^{N} \left(\rho_I \delta I^n_{\ell m} + \rho_w \{ \delta S^n_{\ell m} \}^E \right) \beta(\ell, t_n, t) H(t - t_n) Y_{\ell m} \right] \tag{51}$$

where, following equation (11),

$$\frac{\Delta \Phi^E(t)}{g} = -\frac{M_I(t)}{\rho_w A_o} - \frac{1}{A_o} < \sum_{\ell,m} E_\ell T_\ell \left(\rho_I I_{\ell m}(t) + \rho_w S^E_{\ell m}(t) \right) Y_{\ell m} > - \frac{1}{A_o} < \sum_{\ell,m} T_\ell \sum_{n=o}^{N} \left(\rho_I \delta I^n_{\ell m} + \rho_w \{ \delta S^n_{\ell m} \}^E \right) \beta(\ell, t_n, t) Y_{\ell m} > . \tag{52}$$

Furthermore, the total and incremental eustatic ocean loads (denoted by the supercript E) are given by (following equation (49))

$$S^E_{\ell m}(t) = - \left\{ \frac{\rho_I}{\rho_w} \frac{4\pi a^2}{A_o} I_{oo}(t) \right\} C_{\ell m}$$

$$\{ \delta S^n_{\ell m} \}^E = - \left\{ \frac{\rho_I}{\rho_w} \frac{4\pi a^2}{A_o} \delta I^n_{oo} \right\} C_{\ell m} . \tag{53}$$

Since all parameters on the right-hand side of equation (51) are known, the solution of the equation, for the harmonics of the sea level change $S'_{\ell m}$ (which represent an approximation to the gravitationally self-consistent harmonics $S_{\ell m}$) is straightforward. The approximation has, for example, been adopted by *Nakada and Lambeck* [1987, 1989]; however, these authors generalized the time dependence of the ice loading history by incorporating a linear deglaciation history between each time interval (rather than an instantaneous increment as described by equation (14)).

A second, even less accurate approximation, is the so-called "eustatic approximation" [*Wu and Peltier*, 1983]. Once again, the technique assumes that meltwater loads the ocean eustatically; however, it also assumes that changes in sea level are only produced by the radial displacement of the solid surface and variations in the eustatic ocean bathymetry produced by the deglaciation. In this case the governing equation is

$$\sum_{\ell,m} S^*_{\ell m}(t) Y_{\ell m} = \left\{ \sum_{r,s} C_{rs} Y_{rs} \right\} \left[\frac{\Delta \Phi^*(t)}{g} + \sum_{\ell,m} E^*_\ell T_\ell \left(\rho_I I_{\ell m}(t) + \rho_w S^E_{\ell m}(t) \right) Y_{\ell m} + \sum_{\ell,m} T_\ell \sum_{n=o}^{N} \left[\rho_I \delta I^n_{\ell m} + \rho_w \{ \delta S^n_{\ell m} \}^E \right] \beta^*(\ell, t_n, t) H(t - t_n) Y_{\ell m} \right] \tag{54}$$

where

$$\frac{\Delta \Phi^*(t)}{g} = - \frac{M_I(t)}{\rho_w A_o}$$

$$E^*_\ell = - h^E_\ell \tag{55}$$

$$\beta^*(\ell, t_n, t) = \sum_{k=1}^{K} \frac{-r^\ell_k}{s^\ell_k} \left[1 - \exp(-s^\ell_k (t - t_n)) \right] .$$

In section 4.2 we consider, in detail, RSL variations in the far field of the Pleistocene ice sheets computed using the pseudo-spectral formalism. Within this context the accuracy of the two gravitationally self-consistent techniques described in this section will also be assessed.

4. RESULTS

A solution of the sea level equation requires, as input, both the radial visco-elastic structure of the planet and the history of the surface ice load. In the analysis below we will assume, as in previous studies [e.g., *Wu and Peltier*, 1983], that the last glaciation phase of the current ice age was of sufficient duration that a condition of isostatic equilibrium prevailed at the onset of the deglaciation phase 18 kyrs before present (B.P.) on the ^{14}C time scale. Some justification for this assumption was provided by *Wu and Peltier* [1983]. Results to be described in a companion paper (J.X. Mitrovica and W.R. Peltier, manuscript in preparation, 1991) indicate that the assumption is valid for the relatively recent RSL changes with which we will be concerned in this study.

In recent years models of late Pleistocene deglaciation, constructed using constraints imposed by steady state ice mechanics and geological end moraine data [*Peltier and Andrews*, 1976], have been refined on the basis of their ability to predict observed RSL changes [*Wu and Peltier*, 1983; *Tushingham and Peltier*, 1991]. In our analysis the spherical harmonic coefficients

of the ice load (deglaciation) increments, $\delta I^n_{\ell m}$ (see equations (14*a*) and (21)), will be computed using the ICE-3G model of *Tushingham and Peltier* [1991], in which the deglaciation phase, modelled with a 1-kyr discretization (which we adopt), is assumed to have ended about 4 kyr B.P.

The Earth models employed in this study all have the elastic structure of the seismic model PREM [*Dziewonski and Anderson*, 1981]. They also have a 120-km elastic lithosphere, isoviscous upper and lower mantle regions, and an inviscid core. There is general agreement from previous rebound studies [*Haskell*, 1936; *Peltier*, 1974; *Cathles*, 1975] as well as from investigations of the geoid signal due to convective circulation in the Earth's mantle [*Forte and Peltier*, 1987], that the upper mantle viscosity (ν_{UM}) is very near 10^{21} Pa s, and we therefore adopt this value. The viscosity in the lower mantle region (ν_{LM}) is, however, a point of some contention, so we will consider a range of values extending from the isoviscous mantle case ($\nu_{LM} = \nu_{UM} = 10^{21}$ Pa s) to an extreme value of 10^{25} Pa s.

As described in the introduction, the results outlined in this section will be concerned, primarily, with the present-day rate of RSL change. We have computed this rate, for a particular Earth model, by solving for the sea level increment δS over a very small interval Δt in time (Δt = 10 yrs) straddling the present. We then have

$$\left.\frac{\partial S}{\partial t}\right|_{t=t_p} \approx \frac{\delta S}{\Delta t} . \tag{56}$$

We note here that a useful, and successful, check on the numerical schemes consisted of comparing results generated using the two independent formalisms described in sections 3.1 and 3.2 at a consistent truncation level. We have also found that we were able to accurately reproduce the global map of present-day RSL change published by *Peltier and Tushingham* [1989, Fig. 3] (which was computed using the finite element formulation mentioned in section 2) by using the pseudospectral formulation up to degree 128. The validity and accuracy of this previous finite element formulation is thus also confirmed.

4.1. Computing Low-Degree Sea Level Changes Using the "Full Spectral" Formalism

The output of the formalisms outlined in section 3, for the solution of the sea level equation, are the spherical harmonic coefficients of the sea level increment at each time interval ($\delta S^n_{\ell m}$). Combining these with the ice load increments $\delta I^n_{\ell m}$ generates the total surface load (see equations (12) and (14)). The degree ℓ and order m component of the total load will excite an Earth response which is limited to the same degree and order, and this suggests that the full spectral formalism might be a particularly useful technique for determining the gravitationally self-consistent low-degree signal of the Earth response. An obvious example would be the low degree zonal harmonics in the expansion of the present-day secular variation of the Earth's geoid (J_2, J_3, and J_4), which represent an important data set in inferences of mantle viscosity [*Peltier*, 1983, 1985; *Mitrovica and Peltier*, 1989].

An accurate determination of the harmonics J_ℓ ($\ell \leq 4$) requires that the truncation level D_{MAX} used in the calculations (equations (33)) is sufficiently high to ensure convergence of the computed sea level harmonics in this low-degree range. To investigate this convergence, consider Figure 2 which shows the percentage error in the computation of various zonal harmonics of the present-day rate of sea level change as a function of the truncation level. One should note, in this context, that the specified truncation level is used in all previous time steps, not just the last. The Earth model used in the computations has a factor of 4.5 jump in viscosity across the boundary between the upper and lower mantle although this is somewhat high according to analyses of the sea level record [*Tushingham and Peltier*, 1991, also submitted manuscript,

The results shown indicate that the zonal harmonics for degrees $\ell \leq 4$ have essentially converged for truncation levels near 30. Indeed, the error in the computation of these harmonics is less than 0.25% for $D_{MAX} = 30$. The error in the non-zonal harmonics (not shown), at the same degrees, is comparable. We have found that for $D_{MAX} = 30$, the error does not exceed 5% in the degree range $\ell < 13$. At $\ell = 10$, for example, it is only 2%. We can conclude therefore that the "full spectral" formulation for the solution of the sea level equation can be used to accurately compute the low-order signal in the redistribution of ocean water since the onset of the late Pleistocene deglaciation event. The application of the technique to a gravitationally self-consistent calculation of J_ℓ for $\ell \leq 4$, will be described in a subsequent publication.

4.2. Pleistocene Deglaciation and the Present-Day Rate of Sea Level Change: The Pseudospectral Approach

A global map of the present-day rate of sea level change, computed using the pseudospectral formalism with truncation at degree and order 128, and an Earth model with $\nu_{LM} = 4.5 \times 10^{21}$ Pa s (as in Figure 2), is shown in PLATE 1*a*. The map is not projected onto the ocean function, and therefore it represents the difference between the present-day rate of change of the ocean equipotential surface (the geoid) and the Earth's solid surface. Global maps of each of these contributing fields are shown in Plates 1*b* and 1*c*.

Let us consider, first, the present-day rate of displacement of the Earth's solid surface (Plate 1*b*). Regions once covered by ice sheets (Canada, Greenland, Scandinavia, the Antarctic, etc.) are now characterized by substantial rebound, and for the solution shown in Plate 1*b* the peak uplift rate is 22 mm/yr near the center of Hudson's Bay (this is somewhat in excess of the observed rate in this region). In contrast, the maximum subsidence occurs at the periphery of the deglaciation centers, over the crest of the glacial forebulge [e.g., *Peltier*, 1982]. Indeed, there are several regions on the Earth's surface where the computed subsidence of the forebulge reaches 4mm/yr in Plate 1*b*.

The late Pleistocene deglaciation event, as modelled by the ICE-3G chronology [*Tushingham and Peltier*, 1991*a*], produced a net eustatic sea level rise which exceeded 100m. The effect of this ocean loading is evident in the far field of the Pleistocene ice sheets (that is, beyond the glacial forebulge), where the solid surface displacement is characterized by a weak subsidence in the ocean basins (a response to the additional ocean mass), and a comparably weak uplift of the continents. The uplift is a consequence of the "levering" mechanism supported by the subsidence. That is, in the far field, the continent bearing lithosphere (which is not subjected to a surface load) is flexing upwards due to the downward motion of the surrounding oceanic regions and the transfer of material from the region below the oceanic lithosphere to beneath the continents. The same process has been modelled and discussed by *Clark et al.* [1978] and *Peltier et al.* [1978], who were the first to recognize its global

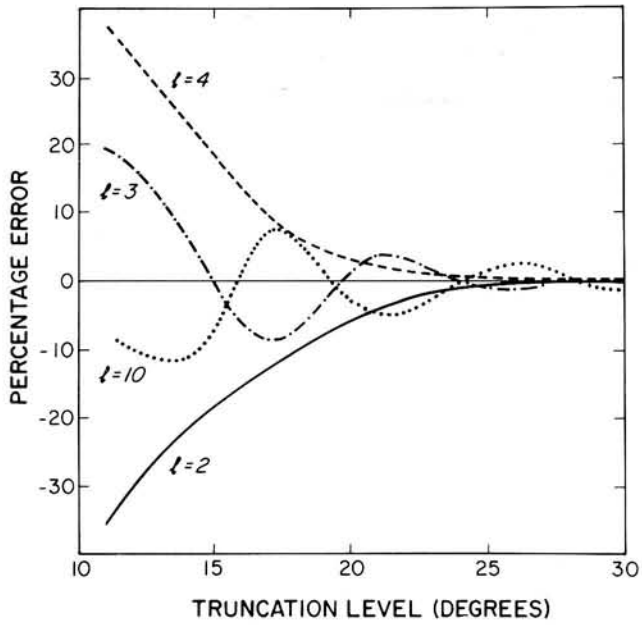

Fig. 2. The percentage error in the calculation of various zonal (m=0) harmonics in the expansion of the present-day rate of sea level change, as a function of the spherical harmonic truncation level, using the full spectral approach outlined in section 3.1. As labelled, the profiles reflect results for degrees 2, 3, 4 and 10. The percentage error is computed using $(\delta S_\ell^c - \delta S_\ell^A)/\delta S_\ell^A$ where the superscript c denotes the computed value and A the value generated using the pseudospectral formulation up to ℓ =128 (which is assumed to be exact for these low degrees). The Earth model has ν_{LM} = 4.5 x 10^{21} Pa s (see section 4).

implications. *Nakada and Lambeck* [1989] have noted the impact of this process in the coastal regions off Australia. Notice that, consistent with the mechanism, the maximum subsidence rate in the far field oceans occurs at the periphery of the continents. Beyond this periphery the subsidence is less than 0.5 mm/yr, and generally much smaller than this in the equatorial oceans.

The global map for the present-day rate of change in the computed geoid (Plate 1*c*) exhibits an uplift in previously glaciated regions and a subsidence elsewhere. In the near field of the ancient ice sheets (including the periphery) the amplitude of the change is only a small fraction of the rate at which the solid surface is deforming. As a consequence, the sea level change in these regions is governed, to a dominant degree, by the latter. This leads to a fall in sea level roughly within the perimeter of the ice sheets and a rise in sea level within the glacial forebulge (notice, given the reversal in sign of the color map, the strong similarity between Plate 1*a* and 1*b* in the near field).

The amplitude of the computed rate of change in the geoid and solid surface is comparable only in the far field. Indeed, the far-field ocean surface is seen to be subsiding, in Plate 1*c*, at a rate near 0.5 mm/yr; which is larger than the rate of subsidence of the ocean floor in this region. The net effect, evident in Plate 1*a*, is a drop in sea level (ocean bathymetry). The fall in sea level over the continents is even larger since the geoid subsidence is met, simultaneously, with an uplift of the land.

We can conclude from these results that the time dependent deformation of the solid surface is the dominant contributor to the near-field present-day sea level changes due to glacial isostatic adjustment. In contrast, the subsidence of the ocean surface (geoid) in the far field is an important factor in the present-day sea level variations in these regions; indeed, the phenomenon governs the sign of the bathymetry change in the bulk of the equatorial ocean. While the physical cause of the solid surface adjustment is clear, the origin of the computed fall in the geoid in the far field is not. What is causing water to leave the equatorial ocean? Furthermore, is the phenomenon a function of the Earth model used in the sea level equation?

To address the latter question we show, in Plate 2, global maps of the present-day rate of sea level change for three different Earth models, distinguished by the value of lower mantle viscosity. We consider in Plates 2*a*, 2*b*, and 2*c* the cases $\nu_{LM} = 10^{21}$ Pa s (an isoviscous mantle), 10^{22} Pa s, and 10^{25} Pa s, respectively. It is clear that even for the extreme range of Earth models considered in Plate 2 the glacial isostatic adjustment process induces a present-day fall in sea level over most of the surface of the equatorial oceans.

The peak amplitude of the computed bathymetry fall in the far field is largest for intermediate values of ν_{LM} (consider, for example, Plates 1*a* and 2*b*), and it diminishes appreciably when the lower mantle viscosity of the Earth model is either reduced to the upper mantle value (Plate 2*a*) or increased to very large values (Plate 2*c*). The cause for this trend will be described below, however it reflects a model dependent variation in the difference between the rates of subsidence of the geoid and solid surface in the far field. Indeed, in the case of Plates 2*a* and 2*c*, the rate of subsidence of the geoid is sufficiently slow in the far field that it is, in fact, smaller than the rate of solid surface subsidence at the perimeter of the continents. The result is a region of sea level rise encircling these continents, a characteristic evident in the solutions of *Peltier* [1988] and *Peltier and Tushingham* [1989] (for models with a lower mantle viscosity of 2 x 10^{21} Pa s).

The nature and variation of the present-day sea level change in the far field is clearly intimately related to the adjustment of the geoid in that region. As described in section 2, the geoid anomaly is comprised of two terms. The first is the time and space dependent position of the original sea level equipotential of the unperturbed Earth, and the second is a term, independent of geography, which ensures that mass is conserved ($\Phi(\theta, \psi, t)/g$ and $\Delta\Phi(t)/g$, respectively; see equation (2)). In the context of Plate 1*c* we have found that the present-day rate of change of the latter is approximately -0.5 mm/yr, which is sufficient to account for the sign of the sea level change over almost the entire equatorial ocean (the only exception is the bathymetry change near the equatorial Pacific ocean which has a computed value slightly higher than -0.5 mm/yr). The term $\Delta\Phi(t)/g$ may therefore provide evidence as to the physical cause of the computed present-day sea level fall in this region, and it is shown, together with the contributions defined in equation (11), in Figure 3.

The dashed curve in Figure 3*a* represents the eustatic sea level variation (equation (11)) for the ICE-3G deglaciation chronology during the last 18 kyr. The curve increases monotonically during the deglaciation period (18 to 4 kyr B.P.); however, the most rapid melting takes place between 14 and 8 kyrs B.P. In the last 4 kyr (a period of no further melting) in the model the total eustatic sea level change remains constant at approximately 110 m.

The three additional terms contributing to $\Delta\Phi(t)/g$ (see equation (11)) are shown in Figure 3*b*. As discussed in section 2, perturbations in the position of the original sea level equipotential surface are produced by the direct attraction of the (time dependent) surface loads and by mass redistributions. The dashed-dotted curve in Figure 3*b* represents an integrated (over the ocean function) measure of the former ($\Delta\Phi^L(t)/g$ in equation (11)), while the dashed curve is a similar measure of the latter ($\Delta\Phi^{MR}(t)/g$ in equation (11)). Similarly, the dotted curve in Figure 3*b* represents the (negative of the) variation in the mean value of

the solid surface displacement over the oceans ($\Delta\Phi^{\Gamma}(t)/g$ in equation (11)). Not surprisingly, the general form of $\Delta\Phi^{L}(t)/g$ is similar to the eustatic sea level variation. In contrast, the terms $\Delta\Phi^{MR}(t)/g$ and $\Delta\Phi^{\Gamma}(t)/g$ exhibit some important differences. In particular, both show variations which persist beyond the deglaciation phase: Indeed, the present-day variations in $\Delta\Phi^{MR}(t)/g$ and $\Delta\Phi^{\Gamma}(t)/g$ in Figure 3 are approximately -0.1 mm/yr and -0.56 mm/yr, respectively. The difference between the two (0.46 mm/yr) accounts for the present-day variation in $\Delta\Phi(t)/g$ evident in Figure 3a and discussed above.

As defined in equation (11), the conservation of mass component $\Delta\Phi(t)/g$ (solid curve Figure 3*a*) is generated by combining the four remaining curves in the figure. During the deglaciation episode, the dominant contributor is the eustatic sea level variation; however, in the last 4 kyr it is the terms $\Delta\Phi^{\Gamma}(t)/g$ and $\Delta\Phi^{MR}(t)/g$, and in particular the former. Recall, we have concluded that the present-day variation in $\Delta\Phi(t)/g$ is sufficient to account for the computed fall in sea level in the far-field oceans. On the basis of Fig. 3 we may further conclude that this fall is a consequence, primarily, of changes in the shape of the planet's solid surface in oceanic regions.

The question still arises as to why the present-day isostatic adjustment of the planet should cause water to migrate from the far field oceans (as in Plates 1*a* and 2). Using the results of Figure 3 we propose the following simple explanation. The onset of the late Pleistocene deglaciation event marked the beginning of the subsidence phase for the forebulge regions at the periphery of the deglaciation centers (note the dark blue shades in Plate 1*b*). It is clear from the color plates that the subsidence persists to the present day and that a large percentage of the glacial forebulges exist within oceanic regions. As a consequence, as the present-day subsidence proceeds, water must inflow into such regions (from both the far field, and the deglaciation centers now undergoing uplift) in order to maintain hydrostatic equilibrium (essentially the ocean mass adjusts to fill the region vacated by the forebulge). This ocean mass redistribution acts to lower the ocean surface or geoid and, once again, the result is a net present-day bathymetry fall in the far field. We have chosen to term the phenomena (of ocean mass flow away from the far field and toward the forebulges) "equatorial ocean syphoning."

The rate of glacial isostatic adjustment over time is a function of the viscoelastic structure of the Earth model, and thus so too must be the strength, as a function of time, of the equatorial ocean syphoning (notice that equatorial ocean syphoning will be presently active on any Earth model). To investigate this we have computed $\Delta\Phi^{\Gamma}(t)/g$ for each of the Earth models used to generate Plates 1 and 2, and the results are shown in Figure 4*a*. Not surprisingly, the curves indicate that the integrated subsidence of the solid surface under the oceans since 18 kyr B.P. decreases monotonically as the lower mantle viscosity of the Earth model is increased.

In the discussion below we will be concerned primarily with the response during the last 4 kyr B.P., after the completion of the ICE-3G deglaciation phase. In that way we avoid consideration of the direct gravitational effect on the ocean system of the massive redistribution of the surface load. In addition, the transfer of mass (from ice sheets to ocean) produces a nonnegligible deformation of the solid surface even in the far field, and hence within this time period the variation in $\Delta\Phi^{\Gamma}(t)/g$ cannot, even approximately, be equated with the strength of any equatorial ocean syphoning which will be acting on the system. Within the last 4 kyr, however, an approximate measure of the strength of the syphoning process is given by the time derivative of $\Delta\Phi^{\Gamma}(t)/g$ ("approximate" primarily because, even in this time period, some deformation of the solid surface will be occurring in the far field). We have computed this time derivative, and the results are shown in Figure 4*b*.

The form of the curves in the figure is extremely significant. The characteristic relaxation time of the Earth model increases as the lower mantle viscosity is increased. As a consequence, while the strength of the syphoning at 4 kyr B.P. is relatively high for the Earth model with $\nu_{LM} = 10^{21}$ Pa s (solid curve), the same model will exhibit a weak present-day syphoning since it will have experienced substantial recovery since the end of deglaciation and will be comparatively close to isostatic equilibrium. At the opposite extreme, models with very high lower-mantle viscosities are characterized, by virtue of their very slow adjustment, by relatively weak equatorial ocean syphoning at all stages during the last 4 kyr. As a consequence, peak present day rates of equatorial ocean syphoning are obtained for models with intermediate values of ν_{LM} (see Figure 4*b*).

These considerations explain why, as described above, the present day far field sea level fall is larger in Plates 1*a* and 2*b* than it is in Plates 2*a* or 2*c* (and why the latter have regions of sea level rise encircling the continents in the far field, while the former do not). To investigate this further, we have computed the mean rate of present-day sea level fall on the equator and the present-day rate of change of $\Delta\Phi^{\Gamma}(t)/g$ (the right intercept of Figure 4*b*), as a function of the lower mantle viscosity of the Earth model. The

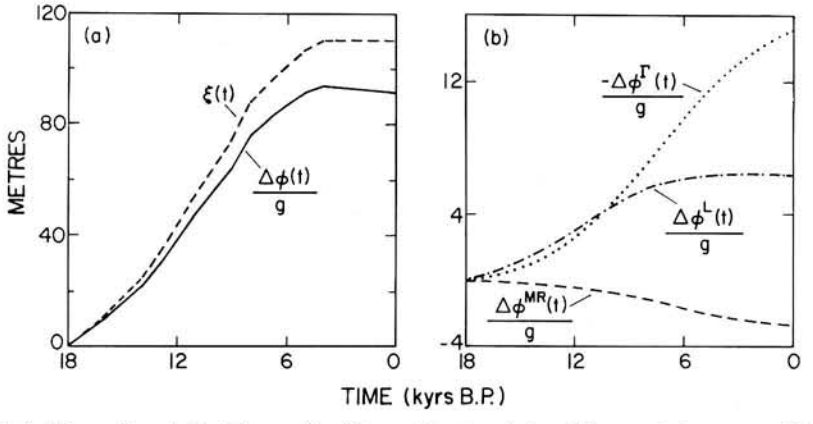

Fig. 3. (*a*) $\Delta\Phi(t)/g$ (solid curve), as defined in equation (6), as a function of time (kiloyears before present) for the Earth model described in section 4 ($\nu_{LM} = 4.5 \times 10^{21}$ Pa s). Also shown are the four contributing terms, $\xi(t)$, $\Delta\Phi^{L}(t)/g$, $\Delta\Phi^{MR}(t)/g$ and $\Delta\Phi^{\Gamma}(t)/g$, defined in equation (11) (see text).

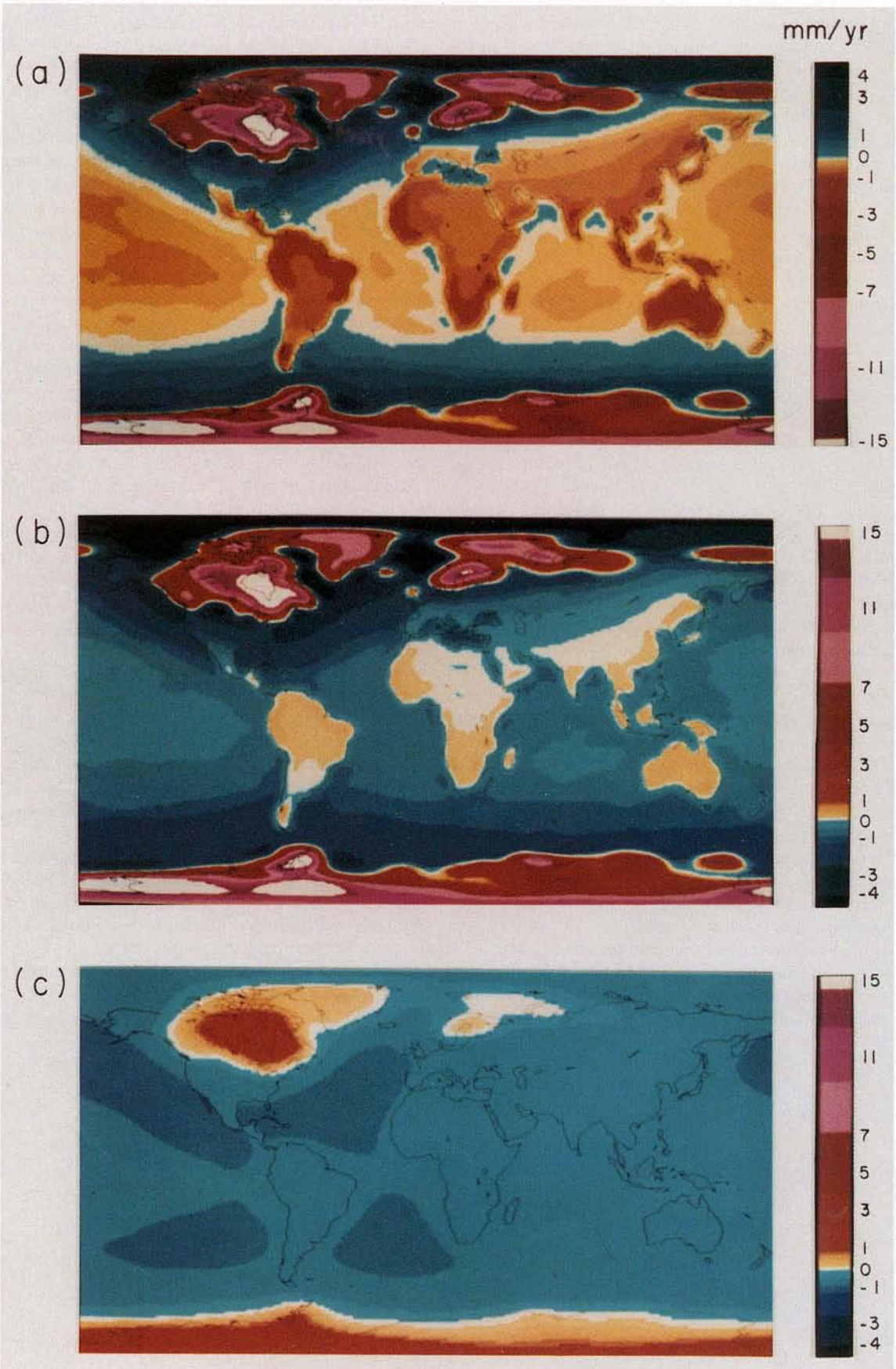

Plate 1. Global maps generated using the Earth model described in section 4, with ν_{LM} = 4.5 x 10^{21} Pa s, and the ICE-3G deglaciation chronology of *Tushingham and Peltier* [1991a]. The maps represent the present-day rates of change in the following fields: (*a*) The sea level (not projected onto the ocean function), the position of the Earth's (*b*) solid surface and (*c*) geoid.

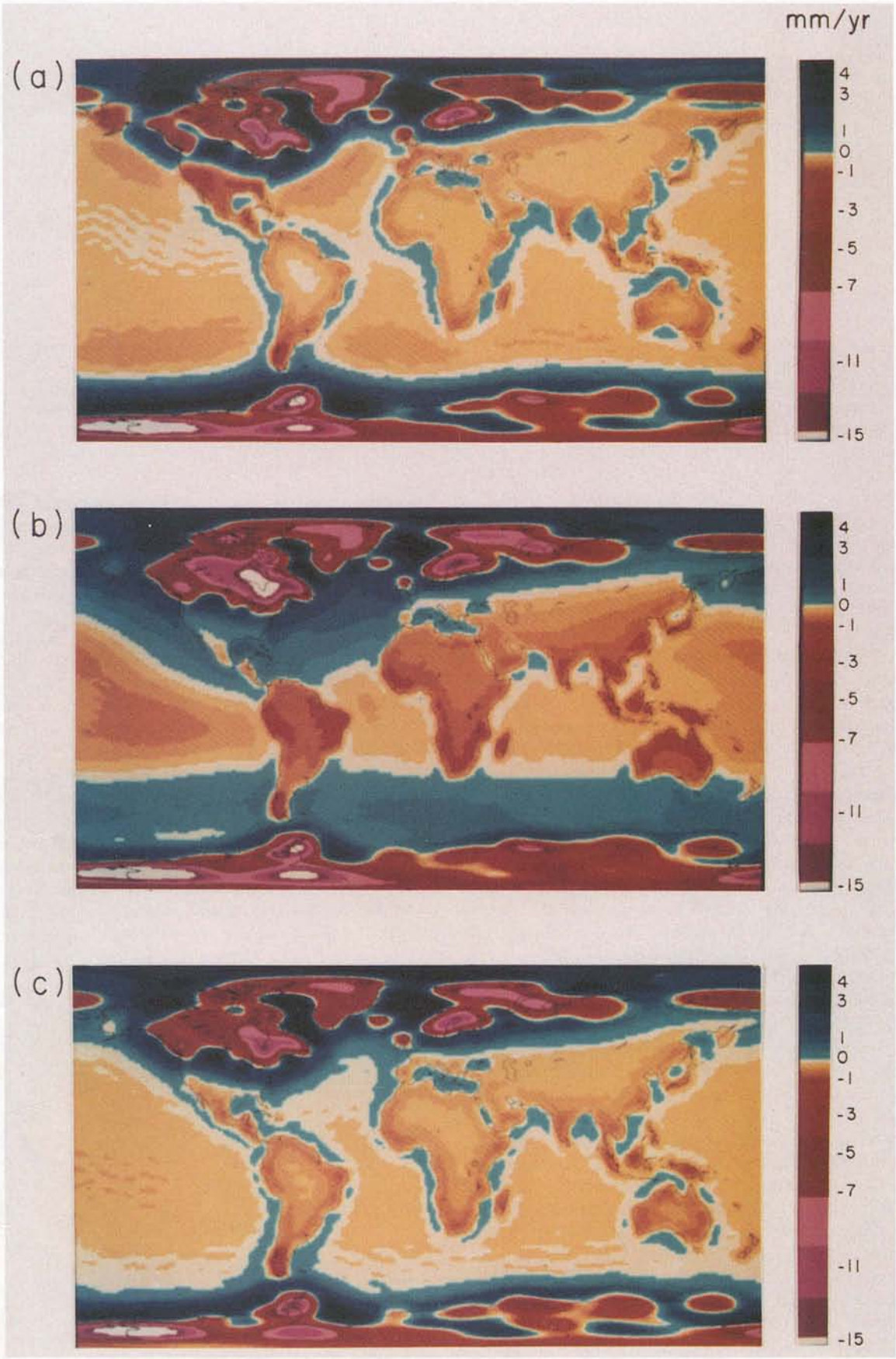

Plate 2. Global maps generated using the Earth model described in section 4 and the ICE-3G deglaciation chronology. The maps represent the present-day rates of change in sea level for models with the following lower mantle viscosities (ν_{LM}): (*a*) 10^{21} Pa s, (*b*) 10^{22} Pa s, and (*c*) 10^{25} Pa s.

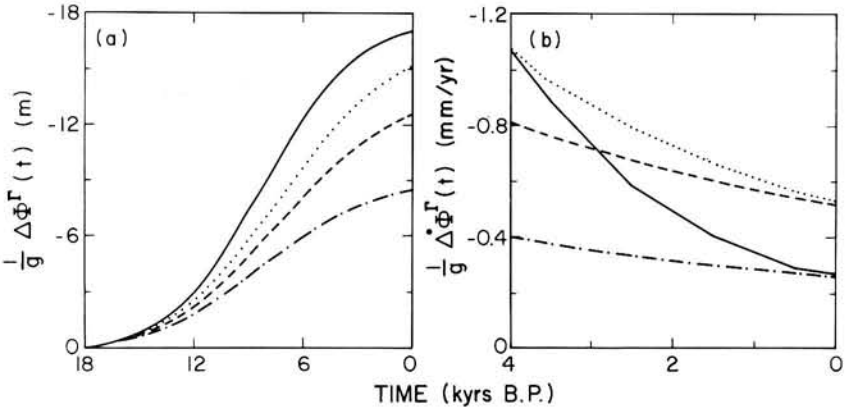

Fig. 4. (a) $\Delta\Phi^{\Gamma}(t)/g$, as defined in equation (11), as a function of time (kiloyears before present) for four different Earth models distinguished by their lower mantle viscosity: $\nu_{LM} = 10^{21}$ Pa s (solid curve), 4.5 x 10^{21} Pa s (dotted curve; as in Figure 3*b*), 10^{22} Pa s (dashed curve), and 10^{25} Pa s (dashed-dotted curve). All other features of the Earth model are described in section 4. (b) The time derivative (denoted by a superscript dot) of the curves in Figure 4*a*, that is, $\dot{\Delta\Phi}^{\Gamma}(t)/g$, during the last 4 kyr (that is, subsequent to the end of the ICE-3G model deglaciation phase; note that in this time period $\xi(t)=0$; see Figure 3*a*).

results, shown in Figure 5, exhibit the predicted correlation. Of course, while the present-day far field sea level fall is comparable for models with $\nu_{LM} = 10^{21}$ or 10^{25} Pa s, the results in Figure 4 indicate that the response of such models will diverge drastically at earlier times. This divergence will be apparent when we compute RSL curves over the last 5 kyr for the various Earth models (Figure 7).

The identification of the equatorial ocean syphoning mechanism is of significance because, in the context of the glacial isostatic adjustment process, it is the dominant cause of sea level variations in ocean regions beyond the peripheral bulge of the Pleistocene ice sheets during the last 4 kyr. The eustatic sea level increase between 18 and 4 kyr B.P. (Figure 3*a*) is, however, sufficient to overwhelm any other effects (including syphoning) which may be active in this time interval. To illustrate this transition (for sea level variations prior to and after 4 kyr B.P.) we have plotted, in Figure 6, the computed RSL curve (solid curve) during the last 10 kyr at Malden Island in the equatorial Pacific Ocean. The curve was generated using the pseudospectral formulation up to degree 128 (a truncation level of 64 produced the same results), and therefore it represents the output of a gravitationally self-consistent solution of the sea level equation. The Earth model used in the calculation had a lower mantle viscosity of 4.5 x 10^{21} Pa s (as in Plate 1 and Figure 3). Notice the monotonic rise in sea level prior to 4 kyr B.P., followed by a steady fall in the postdeglaciation phase which is able to reconcile the observational data set.

The age and elevation data shown in Figure 6 are taken from an extensive global data base of RSL histories compiled by A.M. Tushingham and W.R. Peltier (submitted manuscript, 1991). If the observed fall in sea level at Malden Island during the last 3000 years is due to ocean syphoning, then other far-field sites should exhibit similar trends over the same time interval. To investigate this, we have culled from the A.M. Tushingham and W.R. Peltier (submitted manuscript, 1991) data base all sites which include data from the last 4000 years and which meet the following criteria. First, they must be located in the equatorial region bounded by the 30°N and 30°S lines of latitude. This will ensure that the sites are situated outside the peripheral bulge of the ice sheets regardless of the Earth model (see Plates 1 and 2). Second, the sites must be well removed from the continental margins in order to avoid the effects of continental flexure described earlier. Of the 392 sites collected by A.M. Tushingham and W.R. Peltier (submitted manuscript, 1991) only 18 (including Malden Island) satisfy these constraints, and the data from each, over the last 5000 years, are shown (with error bars) in Figures 8*a*-8*r*. A map illustrating the location of the sites, which are all in the Pacific Ocean, is provided in Figure 7.

The data from 14 of the 18 sites in Figure 8 reflect a net sea level fall in the last 3000 years. Only three sites, E. Caroline Islands, Western Samoa, and Oahu (Figures 8*d*, 8*j*, and 8*q*, respectively, which are denoted by the plus symbol in Figure 7), have experienced a sea level rise over the same time period, while the bathymetry change at a final site, Cook Island (Figure 8*k*), is indeterminate. The sea level rise at Oahu is probably due to the cooling and contraction (that is, subsidence) of the lithosphere as it migrates from the hot spot now positioned under Hawaii. Furthermore, the E. Caroline Islands are located on the arc side of the Mariana trench, while Western Samoa is at the northernmost tip of the Tonga trench. One would therefore expect a contribution to the observed sea level variation, at these sites, from the vertical deflection of the lithosphere associated with any recent transient

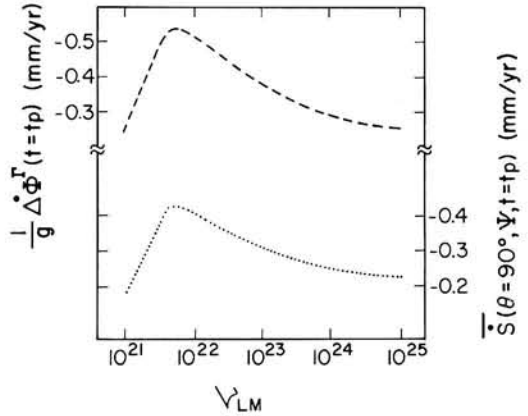

Fig. 5. The present-day ($t=t_p$) value of $\dot{\Delta\Phi}^{\Gamma}(t)/g$ (dashed curve; as in the right intercept of the curves in Figure 4*b*), and the mean (denoted by an overbar) present-day rate of sea level change in ocean regions on the equator (dotted curve), $\bar{\dot{S}}(\theta = 90°, \Psi, t_p)$, as a function of the lower mantle viscosity (ν_{LM}) of the Earth model used in the solution of the sea level equation.

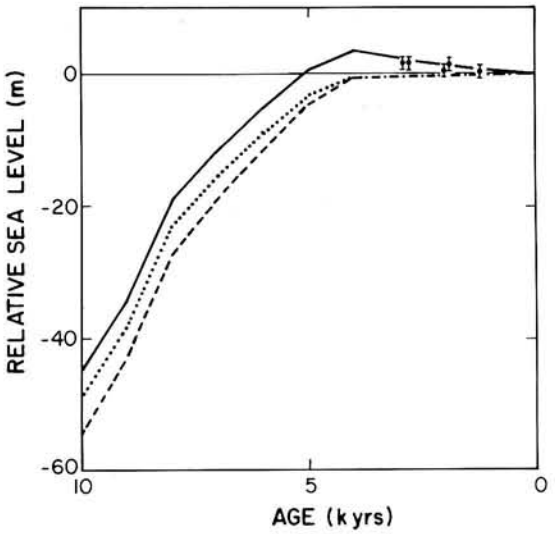

Fig. 6. The predicted RSL variation (solid curve) during the last 10 kyr at Malden Island in the equatorial Pacific Ocean (site o on Figure 7), computed using the pseudospectral approach outlined in section 3.2. The two remaining curves (dotted, dashed) represent solutions to the sea level variation computed using the eustatic approximation (equation (54)), and they are described in detail in the text. All calculations were performed using the Earth model described in Figure 3. The observational data set (5 beaches up to age 2.9 kyr), with error bars (the error in the ages is about ±200 years), is also shown in the figure (see also Figure 8*o*).

dynamics of the adjacent subduction zones [*Mitrovica et al.*, 1989].

Many of the sites in Figure 7 are part of, or adjacent to, seamount chains and hot spot traces. As a consequence they may be susceptible to thermal isostatic or tectonic effects associated with these regions. Nevertheless, the results of Figure 8 indicate that the sea level fall at Malden Island, described in the context of Figure 6 (see also Figure 8*o*), is part of a much larger trend in the far field of the Pleistocene ice sheets during the last few thousand years. It is clear that ocean syphoning is playing a significant role in the bathymetry variations in this region during this time period, and it is logical to ask whether the observed sea level fall might be useful in constraining mantle rheology. To this end, we have predicted the RSL variations at all 18 sites (using the pseudo-spectral technique up to degree 128; once again convergence was established by degree 64) for four different Earth models distinguished on the basis of their lower mantle viscosity (ranging from the isoviscous mantle case, $\nu_{LM} = 10^{21}$ Pa s, to $\nu_{LM} = 10^{25}$ Pa s). The results are shown superimposed on the observations in Figure 8.

The predicted RSL curves in Figure 8 illustrate the time dependent nature of the ocean syphoning mechanism described above. As discussed, the present-day strength of the syphoning is largest for Earth models with intermediate lower mantle viscosity (see Figure 5; notice the present-day slope of the dashed and dotted curve in Figure 8). The Earth model with a very stiff lower mantle viscosity ($\nu_{LM} = 10^{25}$ Pa s, dashed-dotted curve) exhibits a relatively weak syphoning throughout the 4000- year postdeglaciation period. Again, this is a reflection of the slow isostatic adjustment which characterizes the model (see Figure 4*b*). The Earth model with an isoviscous (10^{21} Pa s) mantle also exhibits a weak present-day syphoning because it will have more nearly reached (by today) a state of isostatic equilibrium. At the beginning of the postdeglaciation phase, however, the predicted fall in sea level for this model is much more rapid (notice, in accord with Figure 4*b*, the large slope in the solid curves of Figure 8 between 4 and 2 kyrs B.P.) since the isostatic adjustment of the peripheral bulges (which drives the syphoning) would not yet have slowed.

As a consequence of wave and tidal action, the elevation error in the observed data set has a strict minimum value of ±1m [A.M. Tushingham and W.R. Peltier (submitted manuscript, 1991)]. It is clear from Figure 8 that the sensitivity of the predictions, to the value of ν_{LM}, while explicable in terms of the theory of ocean syphoning described above, is not large compared to this error, even with a 4 order of magnitude change in ν_{LM}. This suggests that data from these far-field sites may not yield particularly reliable estimates of mantle viscosity.

Inferences of mantle rheology based upon these far-field data are also complicated by the fact that the space-time geometry of the Antarctic ice sheet is not particularly well constrained [*Denton and Hughes*, 1981]. Indeed, it is conceivable that there may have been nonnegligible changes in the last 4000 years [*Adamson and*

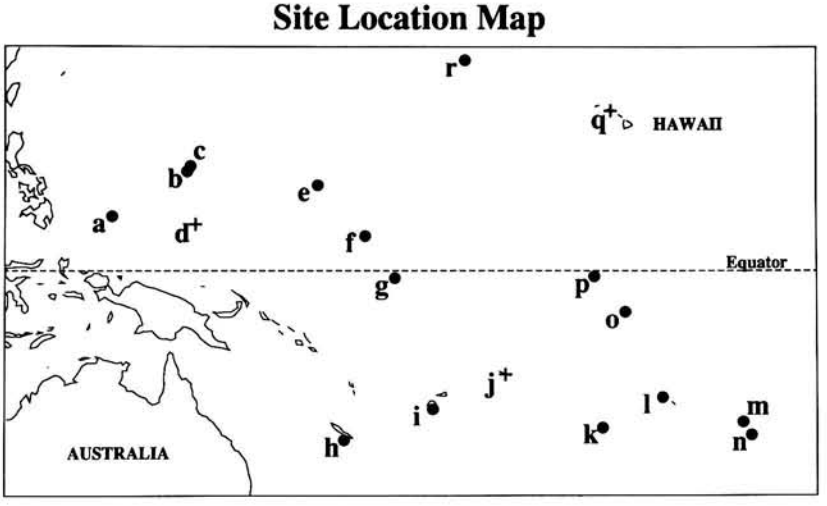

Fig. 7. A map showing the location of the 18 sites included in Figure 8. The labels a through r refer to the site in the analogous frame of Figure 8. The plus symbol distinguishes the three sites (d, j, and q) where the observational data set indicates a net sea level rise in the last 3000 years (see text). The map is bounded by the 30°N and 30°S lines of latitude, and the 120°E and 130°W lines of longitude.

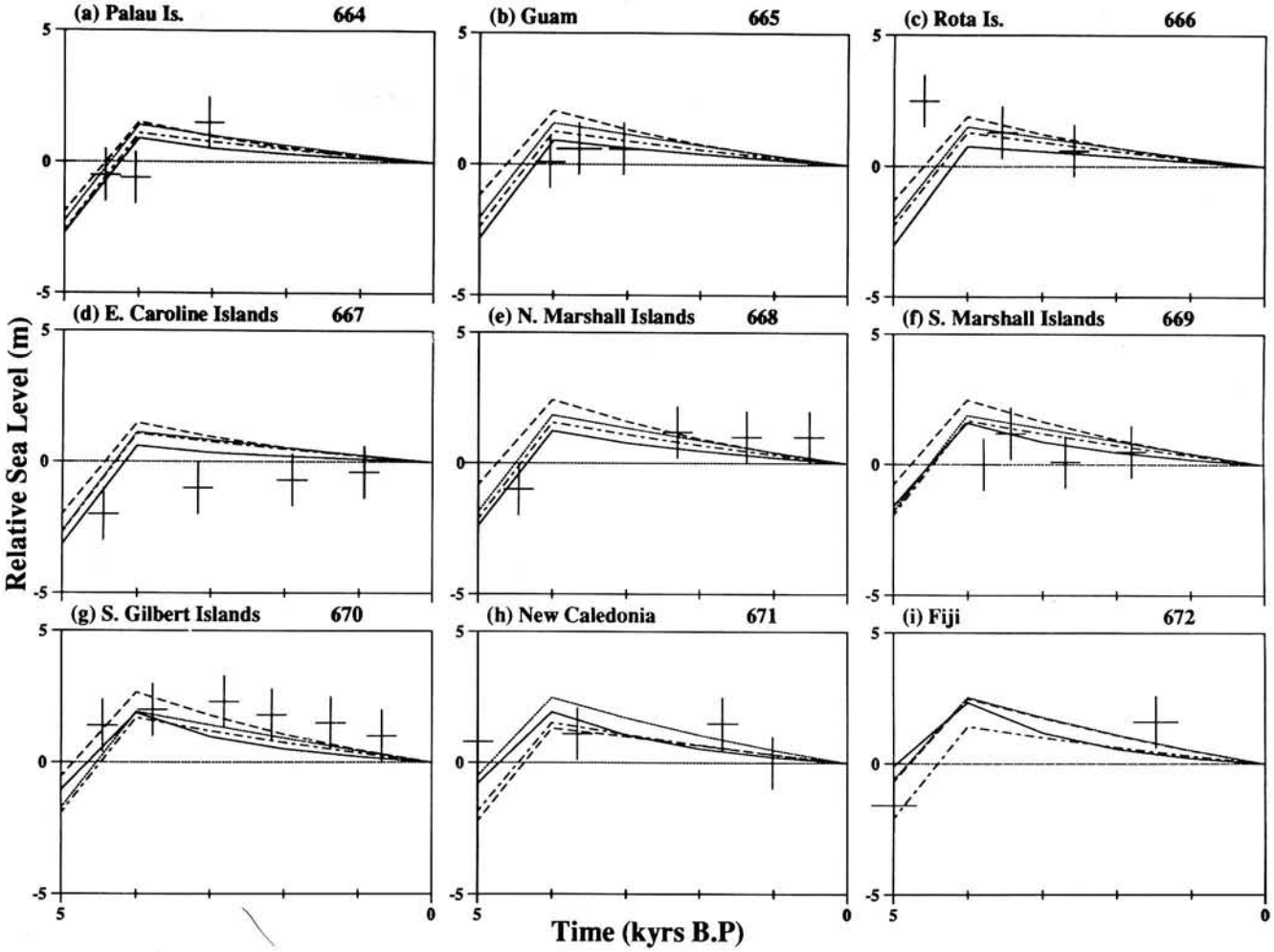

Fig. 8. The observed and predicted RSL variation, during the last 5000 years, at the 18 small Pacific Ocean sites shown on Figure 7. The age and elevation data, together with the error bars, are taken from the data base compiled by A.M. Tushingham and W.R. Peltier (submitted manuscript, 1991) (the number on each frame, beginning at 664 for Palau Island, is the reference number within that data base). The four predicted RSL curves in each frame have been computed using the pseudospectral formalism with a spherical harmonic truncation level of 128, and an Earth model with a lower mantle viscosity of 10^{21} Pa s (solid curve), 4.5 x 10^{21} Pa s (dashed curve), 10^{22} Pa s (dotted curve), and 10^{25} Pa s (dashed dotted curve). All other features of the Earth model are described in section 4.

Pickard, 1986]. In the ICE-3G deglaciation chronology used to compute the RSL curves in Figure 8, the last 4000 years have been modelled as an interglacial period. A small amount of meltwater from the Antarctic ice sheet during this time interval would act to reduce the sea level fall (due to syphoning) in all the computed curves in Figure 8. Given the weak sensitivity of the predicted curves to ν_{LM}, this uncertainty in the recent ice-ocean mass transfer is potentially an important source of error in the inference of rheology.

The sea level fall during the last 3000 years evident in the observational data set does, in any case, place an upper bound on any recent melting of the Antarctic ice sheet. A eustatic sea level rise of more than 1 to 2 m over this time interval would alter the predicted RSL curves (that is, reduce the dominance of ocean syphoning) in a manner such that isostatic adjustment predictions would be incompatible with the observational data set. *Nakada and Lambeck* [1988, 1989] have argued for minor Late Holocene Antarctic melting on the basis of their analysis of far-field RSL data (primarily from Australian and New Zealand coastal sites, but also from a few small Pacific island sites). *Peltier* [1986] has demonstrated, however, that such melting has a RSL signature which is identical to that of an increase in lithospheric thickness so that it is not possible to disentangle these effects unambiguously.

In section 3.3 we outlined two spectral formalisms based upon certain approximations to the sea level equation. To complete this section we will consider the accuracy of the formalisms in predicting the far-field sea level variations described above. As an example, the dashed curve in Figure 6 represents the sea level variation computed using the "eustatic approximation" (equations (54)-(55)) described by *Wu and Peltier* [1983]. Similarly, the dotted curve was generated using the pseudospectral formalism up to 4 kyr B.P. and the eustatic approximation in the subsequent time interval. Recall, the approximate solution assumes that changes in sea level are only produced by the radial displacement of the solid surface and variations in the eustatic ocean bathymetry produced by the deglaciation. Clearly, error has been introduced at all stages in the response. In particular, in the last 4 kyr B.P. the "eustatic approximation" predicts a slightly rising sea level since the ocean basins are weakly subsiding under the weight of the meltwater (as

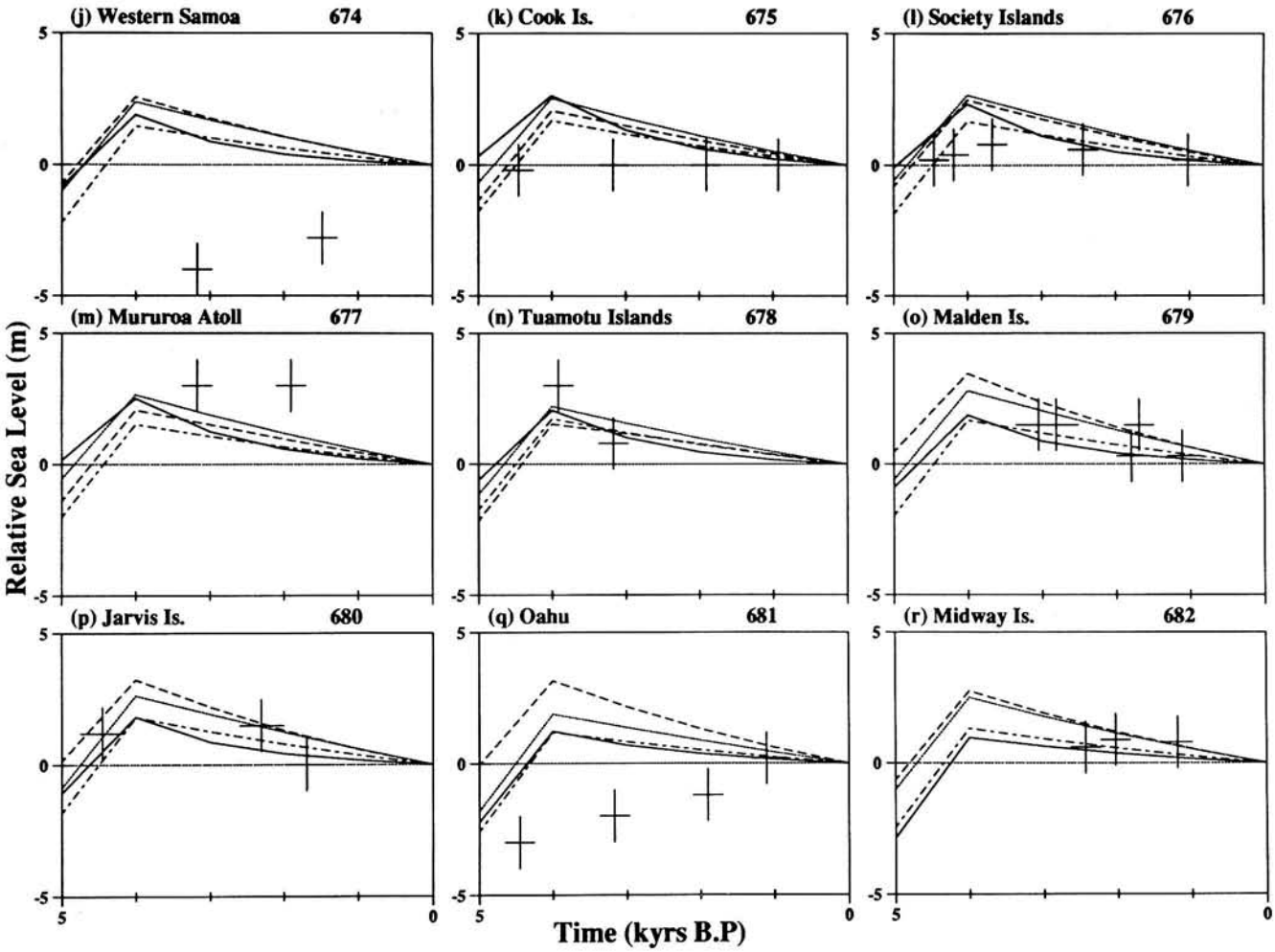

Fig. 8. (continued)

in Plate 1*b*). The term $\Delta\Phi^{*}(t)/g$ in equation (55), since it does not include even an approximation to $\Delta\Phi^{\Gamma}(t)/g$ (equation (11)), cannot, as a consequence, predict the effects of equatorial ocean syphoning. In fact Wu and Peltier did not advocate use of this approximation except in the near field of the ice sheets where it is in fact adequate for some purposes.

In Figure 9 we present RSL curves computed for a subset of far-field sites included in Figures 7 and 8. The solid curve in the figure was generated using the pseudospectral approach and the same Earth model used in Plate 1 (ν_{LM} = 4.5 x 10^{21} Pa s). The dashed curve in Figure 9 shows the results computed using the formulation based on the approximation of *Nakiboglu et al.* [1983] and *Nakada and Lambeck* [1987] (equations (51) to (53)), in which the glacial meltwater is assumed to load the ocean eustatically. Clearly, the latter is a more accurate approach than the "eustatic approximation" when considering far-field RSL variations. Nevertheless, the results in Figure 9 suggest that the error incurred using the *Nakiboglu et al.* [1983] approximation, while dependent on the geographic location of the site, can reach an order of 20% of the true value (which we assume is essentially the same as the pseudospectral solution). Significantly, this error is not small compared to the sensitivity of the computations to even large variations in Earth rheology (Figure 8).

This approximate formalism can nevertheless be modified in order to achieve an accuracy comparable to that obtained using the full pseudospectral approach. To see this consider equation (51), where the coefficients $S'_{\ell m}$ (on the left-hand side) represent the spherical harmonic coefficients of the sea level variation for the approximation of a eustatic ocean loading. In a manner entirely analogous to the derivation of the pseudospectral approach, the coefficients can be "corrected" by solving equation (51) a second time with the following substitutions:

$$S^{E}_{\ell m}(t) \quad \textit{replaced by} \quad S'_{\ell m}(t)$$

$$\{\delta S^{n}_{\ell m}\}^{E} \textit{ replaced by } \{S'_{\ell m}(t_n) - S'_{\ell m}(t_{n-1})\}. \qquad (57)$$

The result is an improved prediction of the true sea level variation. In practice, as in the pseudospectral approach, the procedure can be iteratively repeated to achieve any desired accuracy. As an example, the dash-dotted curve in Figure 9 represents the results for the case of a single correction (equation (57)). In this case the relative error has been reduced to less than 5% with respect to the fully converged pseudospectral solution ($\xi < 10^{-4}$ in equation (50); errors of less than 1% are achieved by applying a second correction).

5. CONCLUSIONS

As discussed in the introduction, RSL changes during the last 18 kyr have, as a manifestation of glacial isostatic adjustment, played a significant role in a variety of geophysical phenomena. In this

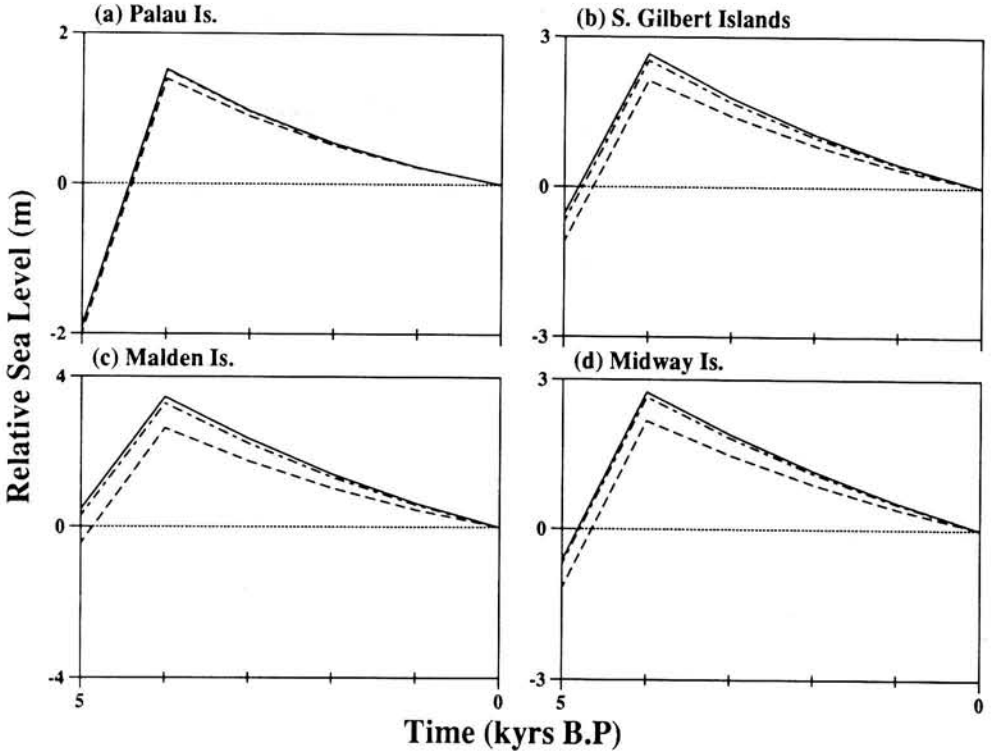

Fig. 9. The predicted RSL variation, during the last 5000 years, at four Pacific Ocean island sites. The solid curve is computed using the pseudospectral approach. The dashed curve is computed using the *Nakiboglu et al.* [1983] approximation which assumes that meltwater loads the ocean eustatically (equations (51)-(53)). The dash-dotted curve is computed by "correcting" the dashed curve in the manner described with respect to equation (57). All calculations used an Earth model with the features described in section 4 with $\nu_{LM} = 4.5 \times 10^{21}$ Pa s and a spherical harmonic truncation level of 128.

respect, the results of the last section indicate that an accurate solution to the equation which governs RSL variations is important in accurately modelling all of the essential features of ocean adjustment evident in the observational data set.

We have, in this context, presented two new techniques for obtaining a gravitationally self-consistent solution of the sea level equation. The "full spectral" formalism (section 3.1) has been shown to be capable of very accurately determining the low degree ($\ell \leq 10$) signal in ocean water redistribution. As a consequence, it will prove especially useful in the gravitationally self-consistent analysis of present-day secular variations in the low degree zonal harmonics of the Earth's geoid (*Peltier*, 1983, 1985; *Mitrovica and Peltier*, 1989]. An accurate prediction of RSL variations at all points on the Earth's surface requires a much higher truncation level, and this is possible using the pseudospectral formalism outlined in section 3.2. Indeed, while the global maps shown in Plates 1 and 2 were computed using a truncation level of 128, an extension of the degree range to 256 (or higher) is feasible.

Using the pseudospectral formalism we have been able to outline a physical theory which explains in detail the present-day global pattern of sea level variations due to glacial isostatic adjustment. In particular, we have identified a mechanism, which we term "equatorial ocean syphoning," that acts to draw water away from the equatorial regions in the far field of the Pleistocene ice sheets. The mechanism is driven by the subsidence of those portions of the glacial forebulges which exist over oceanic regions. As subsidence proceeds, water is forced to inflow into the peripheral regions (from the far field, and near-field regions undergoing uplift) in order that the oceans maintain hydrostatic equilibrium. The net effect is a lowering of the geoid, or ocean surface. The mechanism dominates the RSL variation in ocean regions in the far field of the ice sheets (that is, beyond the peripheral bulge) during periods, such as the last 4 kyr, when the volume of the ice sheets does not change significantly.

It is important to note that equatorial ocean syphoning has been active over the entire far field of the ice sheets, both in the ocean regions away from the continental margins and along such margins. The recent (that is, over the last 3 to 4 kyr) RSL fall evident at small Pacific island sites, such as those shown in Figure 7, and discussed (without explanation) by various authors [e.g., *Clark et al.* 1978; *Peltier*, 1986, *Peltier and Tushingham* 1989; *Nakada and Lambeck*, 1989], is due solely to the syphoning process (with some contamination possible from tectonic processes or minor Late Holocene melting of polar ice sheets or small glaciers). Over the same time period the RSL variation at continental margin sites in the far field is due both to the syphoning mechanism and the continental "levering" process discussed in section 4.2. The contribution of the latter, both in terms of amplitude and sign, will be dependent on the location of the site with respect to the local tilt axis (see Plate 1*b*).

Tide gauge records over the last century indicate the action of an ongoing globally averaged rate of sea level rise of 1 to 2 mm/yr [*Peltier and Tushingham*, 1989], which has been partly attributed to the melting of land-based ice sheets and small glaciers [*Meier*, 1984]. Apparently, this melting is sufficient to have overcome the far-field sea level fall due to syphoning in the same time period (though not on the longer time scale of the last 4000 years; see Figure 8). Nevertheless, it is clear that the ocean syphoning phenomenon cannot be ignored (we have computed present-day rates up to -0.70 mm/yr of sea level change in the far field) when

considering the contributions to the present-day change of global sea level, and, ultimately, their physical origin. Indeed, in the analyses of the tide gauge data presented by *Peltier and Tushingham* [1989, 1991], correction of these data for this and other characteristic features of the global process of postglacial rebound has been shown to significantly reduce the scatter in the secular rates of change that these data reveal.

REFERENCES

Adamson, D. A., and J. Pickard, Cainozoic history of the Vestfold Hills, in *Antarctic Oasis*, edited by J. Pickard, pp. 63-93, Academic, San Diego, California, 1986.

Brussaard, P. J. and H. A. Tolhoek, Classical limits of Clebsch-Gordon coefficients, Racah coefficients, and $D^{4}_{mn}(\phi, \theta, \psi)$ - functions, *Physica*, *23*, 955-971, 1957.

Cathles, L. M., *The Viscosity of the Earth's Mantle*, Princeton University Press, Princeton, N. J., 1975.

Clark, J. A., W. E. Farrell, and W. R. Peltier, Global changes in postglacial sea level: A numerical calculation, *Quat. Res. N.Y.*, *9*, 265-287, 1978.

Cohen-Tannoudji, C., D. Bernard, and F. Laloë, *Quantum Mechanics*, vol. II, John Wiley, New York, 1977.

Dahlen, F. A., The passive influence of the oceans upon the rotation of the Earth, *Geophys. J. R. astron. Soc.*, *46*, 363-406, 1976.

Denton, G. H., and I. J. Hughes (Eds.), *The Last Great Ice Sheets*, Wiley Interscience, New York, 1981.

Dziewonski, A. M. and D. L. Anderson, Preliminary Reference Earth Model (PREM), *Phys. Earth Planet. Inter.*, *25*, 297-356, 1981.

Etkins, R., and E. S. Epstein, The rise of global mean sea level as an indication of climatic change, *Science*, *215*, 287-289, 1982.

Farrell, W. E., Deformation of the Earth by surface loads, *Rev. Geophys.*, *10*, 761-797, 1972.

Farrell, W. E. and J. A. Clark, On postglacial sea level, *Geophys. J. R. astron. Soc.*, *46*, 647-667, 1976.

Forte, A. M., and W. R. Peltier, Surface plate kinematics and mantle convection, in *Composition, Structure and Dynamics of the Lithosphere-Asthenosphere System, Geodyn. Ser.*, vol. 16, edited by K. Fuchs and C. Froidevaux, pp. 125-136, AGU, Washington, D. C., 1987.

Gornitz, V., S. Lebedeff, and J. Hansen, Global sea level trend in the past century, *Science*, *215*, 1611-1614, 1982.

Haskell, N. A., The motion of a viscous fluid under a surface load, 2, *Physics*, *7*, 56-61, 1936.

Laprise, R., The organization and structure of the AES/CCC multi-level spectral general circulation model, *Can. Climate Cent. Rep. 81-8 CCRN-8, Atmos. Environ. Serv.*, Downsview, Canada, 1981.

Le Blanc, R., New perspective on the U(n) Wigner-Racah calculus, III, Applications to U(2) and U(3), *J. Phys. A Math Gen.*, *20*, 5015-5021, 1987.

Meier, M. F., Contribution of small glaciers to global sea level, *Science*, *226*, 1418-1421, 1984.

Mitrovica, J. X., and W. R. Peltier, Pleistocene deglaciation and the global gravity field, *J. Geophys. Res.*, *94*, 13651-13671, 1989.

Mitrovica, J. X. and W. R. Peltier, A complete formalism for the inversion of post-glacial rebound data: Resolving power analysis, *Geophys. J. Int.*, *104*, 267-288, 1991.

Mitrovica, J. X., C. Beaumont, and G. T. Jarvis, Tilting of continental interiors by the dynamical effects of subduction, *Tectonics*, *8*, 1079-1094, 1989.

Munk, W. H., and G. J. F. MacDonald, *The Rotation of the Earth*, Cambridge University Press, New York, 1960.

Nakada, M., and K. Lambeck, Glacial rebound and relative sea level variations: A new appraisal, *Geophys. J. R. Astron. Soc.*, *90*, 171-224, 1987.

Nakada, M., and K. Lambeck, The melting history of the late Pleistocene Antarctic ice sheet, *Nature*, *33*, 36-40, 1988.

Nakada, M., and K. Lambeck, Late Pleistocene and Holocene sea-level change in the Australian region and mantle rheology, *Geophys. J. Int.*, *96*, 497-517, 1989.

Nakiboglu, S. M., K. Lambeck, and P. Aharon, Postglacial sea levels in the Pacific: Implications with respect to deglaciation regime and local tectonics, *Tectonophysics*, *91*, 335-358, 1983.

Peltier, W. R., The impulse response of a Maxwell Earth, *Rev. Geophys.*, *12*, 649-669, 1974.

Peltier, W. R., Glacial-isostatic adjustment, II, The inverse problem, *Geophys. J. R. Astron. Soc.*, *46*, 669-705, 1976.

Peltier, W. R., Dynamics of the ice age Earth, *Adv. Geophys.*, *24*, 1-146, 1982.

Peltier, W. R., Constraint on deep mantle viscosity from LAGEOS acceleration data, *Nature*, *304*, 434-436, 1983.

Peltier, W. R., The LAGEOS constraint on deep mantle viscosity: Results from a new normal mode method for the inversion of viscoelastic relaxation spectra, *J. Geophys. Res.*, *90*, 9411-9421, 1985.

Peltier, W. R., Lithospheric thickness, Antarctic deglaciation history, and ocean basin discretization effects in a global model of postglacial sea level change: A summary of some sources of non-uniqueness, *Quat. Res. N.Y.*, *29*, 93-112, 1986.

Peltier, W. R., Global sea level and Earth rotation, *Science*, *240*, 895-901, 1988.

Peltier, W. R., and J. T. Andrews, Glacial isostatic adjustment, I, The forward problem, *Geophys. J. R. Astron. Soc.*, *46*, 605-646, 1976.

Peltier, W. R. and A. M. Tushingham, Global sea level rise and the greenhouse effect: Might they be connected?, *Science*, *244*, 806-810, 1989.

Peltier, W. R., W. E. Farrell, and J. A. Clark, Glacial isostasy and relative sea level: A global finite element model, *Tectonophysics.*, *50*, 81-110, 1978.

Peltier, W.R., and M.A. Tushingham, The influence of glacial isostatic adjustment on tide gauge measurements of secular sea level change, *J. Geophys. Res.*, *96*, 6779-6796.

Richards, M. A., and B. H. Hager, Geoid anomalies in a dynamic Earth, *J. Geophys. Res.*, *89*, 5987-6002, 1984.

Tushingham, A. M., and W. R. Peltier, ICE-3G: A new global model of late Pleistocene deglaciation based upon geophysical predictions of postglacial relative sea level change, *J. Geophys. Res.*, *96*, 4497-4523, 1991*a*.

Tushingham, A. M. and W. R. Peltier, Constraints on visco-elastic Earth structure from a global data base of late Pleistocene relative sea level histories, *J. Geophys. Res.*, in press, 1991*b*.

Wu, P., and W. R. Peltier, Glacial isostatic adjustment and the free air gravity anomaly as a constraint on deep mantle viscosity, *Geophys. J. R. Astron. Soc.*, *74*, 377-450, 1983.

Wu, P., and W. R. Peltier, Pleistocene deglaciation and the Earth's rotation: A new analysis, *Geophys. J. R. Astron. Soc.*, *76*, 753-791, 1984.

J.X. Mitrovica, Harvard-Smithsonian, Center for Astrophysics, 60 Garden St., MS-42, Cambridge, MA 02138.

W.R. Peltier, Department of Physics, University of Toronto, Toronto, Ontario, Canada M5S 1A7.

(Received May 18, 1990:
revised March 1, 1991;
accepted April 26, 1991.)